Journal of Virology®

PATHOGENESIS AND IMMUNITY

Chikungunya Virus Evades Antiviral CD8$^+$ T Cell Responses To Establish Persistent Infection in Joint-Associated Tissues

Bennett J. Davenport,[a] Christopher Bullock,[b] Mary K. McCarthy,[a] David W. Hawman,[a] Kenneth M. Murphy,[b,f] Ross M. Kedl,[a] Michael S. Diamond,[b,c,d,e] Thomas E. Morrison[a]

[a]Department of Immunology and Microbiology, University of Colorado School of Medicine, Aurora, Colorado, USA
[b]Department of Pathology and Immunology, Washington University School of Medicine, St. Louis, Missouri, USA
[c]Department of Molecular Microbiology, Washington University School of Medicine, St. Louis, Missouri, USA
[d]Department of Medicine, Washington University School of Medicine, St. Louis, Missouri, USA
[e]The Andrew M. and Jane M. Bursky Center for Human Immunology and Immunotherapy Programs, Washington University School of Medicine, St. Louis, Missouri, USA
[f]Howard Hughes Medical Institute, Washington University School of Medicine, St. Louis, Missouri, USA

ABSTRACT Chikungunya virus (CHIKV) is a mosquito-transmitted alphavirus that causes explosive epidemics of a febrile illness characterized by debilitating arthralgia and arthritis that can endure for months to years following infection. In mouse models, CHIKV persists in joint tissues for weeks to months and is associated with chronic synovitis. Using a recombinant CHIKV strain encoding a CD8$^+$ T cell receptor epitope from ovalbumin, as well as a viral peptide-specific major histocompatibility complex class I tetramer, we interrogated CD8$^+$ T cell responses during CHIKV infection. Epitope-specific CD8$^+$ T cells, which were reduced in *Batf3*$^{-/-}$ and *Wdfy4*$^{-/-}$ mice with known defects in antigen cross-presentation, accumulated in joint tissue and the spleen. Antigen-specific *ex vivo* restimulation assays and *in vivo* killing assays demonstrated that CD8$^+$ T cells produce cytokine and have cytolytic activity. Despite the induction of a virus-specific CD8$^+$ T cell response, the CHIKV burden in joint-associated tissues and the spleen were equivalent in wild-type (WT) and CD8$\alpha^{-/-}$ mice during both the acute and the chronic phases of infection. In comparison, CD8$^+$ T cells were essential for the control of acute and chronic lymphocytic choriomeningitis virus infection in the joint and spleen. Moreover, adoptive transfer of virus-specific effector CD8$^+$ T cells or immunization with a vaccine that induces virus-specific effector CD8$^+$ T cells prior to infection enhanced the clearance of CHIKV infection in the spleen but had a minimal impact on CHIKV infection in the joint. Collectively, these data suggest that CHIKV establishes and maintains a persistent infection in joint-associated tissue in part by evading CD8$^+$ T cell immunity.

IMPORTANCE CHIKV is a reemerging mosquito-transmitted virus that in the last decade has spread into Europe, Asia, the Pacific Region, and the Americas. Joint pain, swelling, and stiffness can endure for months to years after CHIKV infection, and epidemics have a severe economic impact. Elucidating the mechanisms by which CHIKV subverts antiviral immunity to establish and maintain a persistent infection may lead to the development of new therapeutic strategies against chronic CHIKV disease. In this study, we found that CHIKV establishes and maintains a persistent infection in joint-associated tissue in part by evading antiviral CD8$^+$ T cell immunity. Thus, immunomodulatory therapies that improve CD8$^+$ T cell immune surveillance and clearance of CHIKV infection could be a strategy for mitigating chronic CHIKV disease.

KEYWORDS CD8 T cell, alphavirus, chikungunya virus, viral persistence

Chikungunya virus (CHIKV) is a mosquito-transmitted, positive-sense, single-stranded RNA virus in the *Alphavirus* genus of the *Togaviridae* family (1). CHIKV was first isolated in 1952 from patient serum samples during an outbreak of febrile illness in

Citation Davenport BJ, Bullock C, McCarthy MK, Hawman DW, Murphy KM, Kedl RM, Diamond MS, Morrison TE. 2020. Chikungunya virus evades antiviral CD8$^+$ T cell responses to establish persistent infection in joint-associated tissues. J Virol 94:e02036-19. https://doi.org/10.1128/JVI.02036-19.

Editor Julie K. Pfeiffer, University of Texas Southwestern Medical Center

Address correspondence to Thomas E. Morrison, thomas.morrison@cuanschutz.edu.

Received 3 December 2019
Accepted 14 February 2020
Accepted manuscript posted online 26 February 2020
Published 16 April 2020

what is now Tanzania (2). Subsequently, CHIKV became recognized as a cause of outbreaks of febrile illness in regions of Africa and Asia that were characterized by acute and often protracted intense musculoskeletal pain and inflammation (2–7). Since 2004, CHIKV has caused numerous large-scale epidemics in humans involving millions of infections in the Indian Ocean region and Southeast Asia, with spread into Europe, the Middle East, and the Pacific region (8–12). In 2013, local transmission of CHIKV occurred in the Western Hemisphere on islands in the Caribbean (13). The virus rapidly spread throughout the Americas, causing more than 1 million infections in more than 48 countries (14, 15).

Acute CHIKV infection is characterized by the rapid onset of high fever with severe joint pain, joint swelling, muscle pain, and rash (16). More severe outcomes, including encephalitis and even death, can occur in neonates and the elderly (17). Remarkably, in some studies, up to two-thirds of individuals infected experience relapsing/episodic or continuous incapacitating arthralgia, arthritis, and tenosynovitis that endure for months to years after the acute phase (18, 19).

The mechanisms by which CHIKV infection leads to chronic musculoskeletal disease are not fully elucidated. Although CHIKV infection is hypothesized to induce autoimmunity, the prevalence of autoimmune markers, such as rheumatoid factor, antinuclear antibodies, and anticitrullinated protein antibodies, in patients with chronic CHIKV disease is absent or low (20–29). Persistent CHIKV infection in joint-associated tissues has also been hypothesized to contribute to chronic CHIKV disease. However, small joints of the wrists, hands, and feet, which are often the primary sites affected in patients with chronic CHIKV disease (16), are not routinely tested for the presence of infectious virus, viral RNA, or viral antigen. Nevertheless, CHIKV antigen and RNA have been detected in synovial and muscle tissue biopsy specimens collected from patients during the chronic phase of disease (30, 31). Additional evidence for CHIKV persistence comes from experiments in animal models. In immunocompetent mice, CHIKV RNA and antigen persist in joint-associated tissues for weeks to months after infection (32–37). In addition, mice infected with a recombinant luciferase-expressing CHIKV strain display luciferase activity as late as 60 days postinfection, and low levels of infectious virus were detected in the joint-associated tissue of adult and aged mice at 60 to 90 days postinfection (35). In CHIKV-infected macaques, joint, muscle, liver, and lymphoid tissues harbor infectious CHIKV or CHIKV RNA for weeks after inoculation (38, 39).

$CD8^+$ T cells are critical for the control and clearance of many viral infections. However, in contrast to humoral immunity, the role of $CD8^+$ T cells during CHIKV infection remains poorly understood. In humans, activated $CD8^+$ T cells circulate during acute and chronic CHIKV disease (22, 30, 40, 41) and are present in muscle and joint tissue biopsy specimens collected from patients with chronic CHIKV disease (30, 31). In one study, the antigenic response profile of $CD8^+$ T cells correlated with disease outcome: recovered patients exhibited a $CD8^+$ T cell response predominantly against the CHIKV E2 envelope glycoprotein, whereas patients with chronic disease had greater responses to the CHIKV nonstructural protein nsP1 (41), suggesting that the pattern of T cell reactivity may influence the clinical outcome.

Similar to human patients, activated $CD8^+$ T cells circulate in nonhuman primates (NHPs) infected with CHIKV (38, 39). Moreover, the magnitude and breadth of these responses were diminished in aged NHPs that developed persistent CHIKV infection (39). In mice, activated $CD8^+$ T cells accumulate in joint-associated tissue during CHIKV and Ross River virus (RRV) infection (42, 43). In the context of RRV infection, the protective capacity of $CD8^+$ T cells was restrained by arginase 1-expressing macrophages in some tissues (44, 45), supporting the idea that suppression of $CD8^+$ T cell responses may promote chronic infection with an arthritogenic alphavirus.

In this study, we used a well-defined mouse model of acute and chronic CHIKV infection, recombinant CHIKV strains encoding ovalbumin (OVA)-specific $CD8^+$ T cell receptor (TCR) epitopes, and newly generated viral peptide-specific major histocompatibility complex (MHC) class I tetramers to investigate the magnitude, kinetics, and function of the $CD8^+$ T cell responses against CHIKV (32, 42). During acute CHIKV

infection, antigen-specific CD8$^+$ T cells accumulated in joint-associated tissues. Priming of these antigen-specific CD8$^+$ T cells occurred by both direct and cross-presenting mechanisms, as antigen-specific CD8$^+$ T cell responses were reduced only moderately in mice with defects in cross-presentation capacity. Functional analyses revealed that antigen-specific CD8$^+$ T cells in joint and lymphoid tissue produce cytokines and have cytolytic capacity. Nevertheless, the complete absence of CD8$^+$ T cells in genetically deficient mice had no effect on the CHIKV tissue burden during the acute or chronic phase of infection, suggesting that CHIKV-specific CD8$^+$ T cells do not contribute to the antiviral response. Lastly, adoptive transfer of effector CD8$^+$ T cells or immunization with a T cell-based vaccine prior to infection accelerated viral clearance in lymphoid tissues but had minimal effects in joint-associated tissue. Taken together, these data suggest that CHIKV establishes and maintains a persistent infection in joint-associated tissue in part by evading CD8$^+$ T cell immunity.

RESULTS

CHIKV infection elicits antigen-specific CD8$^+$ T cell responses. CHIKV(OVA)-AF is a recombinant virus engineered to encode the H-2K^b-restricted ovalbumin $OVA_{257–264}$ epitope (K^bOVA_{257}; SIINFEKL) and the I-A^d/I-A^b-restricted $OVA_{323–339}$ epitope (ISQAVH AAHAEINEAGR) in-frame with the viral structural polyprotein in the genome of the pathogenic CHIKV strain AF15561 (46). Four-week-old wild-type (WT) C57BL/6 male mice were mock inoculated or inoculated via subcutaneous (s.c.) injection with 10^3 PFU of CHIKV(OVA)-AF in the left rear footpad, and CD8$^+$ T cell responses were interrogated during both the acute and the chronic phases at 5, 10, 14, 21, and 28 days postinoculation (dpi). At 5, 10, 14, 21, and 28 dpi, we detected increased numbers of bulk CD8$^+$ T cells in the ipsilateral and contralateral ankles of CHIKV(OVA)-AF-infected mice compared with the mock-inoculated control mice (Fig. 1A). In contrast, CHIKV(OVA)-AF infection marginally increased total CD8$^+$ T cell numbers in the spleen at 14, 21, and 28 dpi. During acute infection (5, 10, and 14 dpi), ~90% of CD8$^+$ T cells in the ipsilateral and contralateral ankles were CD44^{hi} (Fig. 1B), suggesting an antigen-experienced, activated phenotype (47). At late time points (21 and 28 dpi), ~50 to 60% of CD8$^+$ T cells in the ipsilateral and contralateral ankles remained CD44^{hi} (Fig. 1B). CHIKV(OVA)-AF infection also resulted in CD8$^+$ T cell activation in the spleen (Fig. 1B), but as expected, the frequency of CD44^{hi} CD8$^+$ T cells among total CD8$^+$ T cells was lower than that in joint-associated tissues. The total CD44^{hi} CD8$^+$ T cell numbers increased ~100-fold and ~50-fold in the ipsilateral and contralateral ankles, respectively, whereas a more modest increase of ~3-fold was observed in the spleen (Fig. 1C). To quantify antigen-specific T cells during CHIKV(OVA)-AF infection, cell populations isolated from the joints and spleen were stained with K^bOVA_{257} tetramers (tet). As shown in Fig. 1D to G, CHIKV(OVA)-AF infection resulted in the expansion of SIINKEFL-specific CD8$^+$ T cells in the ipsilateral ankle, contralateral ankle, and spleen during acute infection (10 and 14 dpi), with K^bOVA_{257} tet-positive (tet$^+$) CD8$^+$ T cells representing 26 to 38% of all CD8$^+$ T cells in joint-associated tissues (Fig. 1D and F) and 10% of all CD8$^+$ T cells in the spleen (Fig. 1E and F), with 10- to 1,000-fold increased numbers being seen during this time frame (Fig. 1G). At later times postinoculation (21 and 28 dpi), the number of K^bOVA_{257} tet$^+$ CD8$^+$ T cells decreased in all tissues examined compared with the peak response detected at 10 to 14 dpi (Fig. 1G), consistent with a contraction phase (48, 49).

A prior study in WT C57BL/6 mice identified an immunodominant CD8$^+$ T cell receptor epitope in the CHIKV E1 glycoprotein ($E1_{331–339}$) but did not identify its MHC restriction (50, 51). We used an MHC class I stabilization assay to assess the H-2D^b and/or H-2K^b restriction of the $E1_{331}$ peptide (D^bE1_{331} and K^bE1_{331}, respectively) (52). C57BL/6 RMA-S lymphoma cells, which are deficient in the transporter associated with antigen processing 2 (*TAP2*) (53, 54), were cultured overnight at 27°C to promote the accumulation of empty H-2D^b and H-2K^b MHC class I molecules on the cell surface. The RMA-S cells were then pulsed with the CHIKV $E1_{331–339}$ (HSMTNAVTI) peptide for 5 h at 37°C. As controls, RMA-S cells were also pulsed with $OVA_{257–264}$ (SIINFEKL), an H-2K^b-restricted peptide (55, 56); lymphocytic choriomeningitis virus (LCMV) $NP_{396–404}$ (FQP

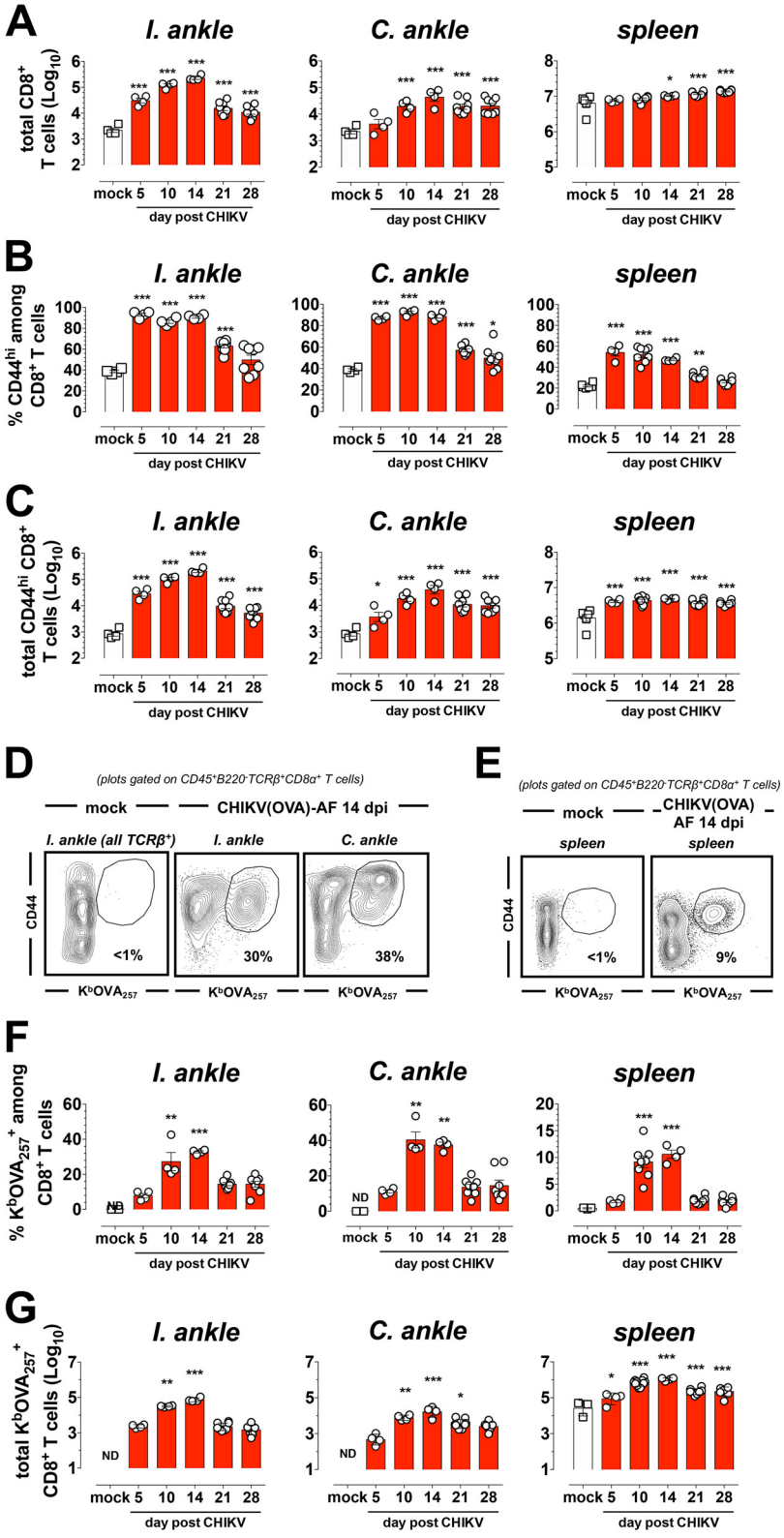

FIG 1 Antigen-specific CD8$^+$ T cells accumulate in joint-associated tissue during CHIKV(OVA)-AF infection. WT C57BL/6J mice (n = 3 to 8 mice/group) were inoculated in the left foot with PBS (mock) or 10^3 PFU of CHIKV(OVA)-AF. At the indicated day postinoculation (dpi), leukocytes were isolated from the ipsilateral (I.) ankle, contralateral (C.) ankle, or spleen and CD8$^+$ T cells were quantified by flow cytometry. (A) Total CD8$^+$ T cells (CD45$^+$ B220$^-$ TCRβ^+ CD8α^+). (B and C) Frequency (B) and total numbers (C) of CD8$^+$ T cells showing an activated phenotype (CD45$^+$ B220$^-$ TCRβ^+ CD8α^+ CD44^{hi}). (D and E) Representative flow cytometry plots showing antigen-specific CD8$^+$ T cells in the ipsilateral ankle and

(Continued on next page)

QNGQFI), an H-2D^b-restricted peptide (57); or LCMV GP_{33-41} (KAVYNFATC), an H-2D^b- and H-2K^b-restricted peptide (58, 59). Next, peptide-mediated MHC class I stabilization was quantified by staining RMA-S cells with anti-mouse H-2D^b (Fig. 2A) or H-2K^b (Fig. 2B) antibodies. As expected, incubation of RMA-S cells harboring empty MHC class I with the $NP_{396-404}$ peptide increased the cell surface levels of H-2D^b (Fig. 2A) but not the levels of H-2K^b (Fig. 2B) compared with those in no-peptide control cells. Similarly, incubation of RMA-S cells harboring empty MHC class I with the $OVA_{257-264}$ peptide increased the cell surface levels of H-2K^b (Fig. 2B) but not H-2D^b compared with those in the no-peptide control cells. Lastly, as expected, incubation of RMA-S cells with the GP_{33} peptide stabilized H-2D^b and, to a lesser degree, H-2K^b (Fig. 2A and B). Incubation of RMA-S cells with the $E1_{331-339}$ peptide strongly increased the cell surface expression levels of H-2D^b but not those of H-2K^b (Fig. 2A and B). Thus, although a prior study utilized K^{b}E1$_{331}$ pentamers to evaluate CHIKV-specific CD8$^+$ T cell responses (60), our data indicate that the CHIKV $E1_{331-339}$ epitope is predominantly H-2D^b restricted. Based on these data, we acquired D^{b}E1$_{331}$ tetramers to track CHIKV-specific CD8$^+$ T cell responses. Similar to CHIKV(OVA)-AF infection, we detected the expansion of D^{b}E1$_{331}$ tet$^+$ CD8$^+$ T cells in joint-associated tissue and the spleen of CHIKV-AF-infected mice (Fig. 2C to F), although these were reduced in frequency and magnitude compared with the frequency and magnitude of the OVA_{257}-specific CD8$^+$ T cell response during CHIKV(OVA)-AF infection (Fig. 1C to F). Collectively, these data suggest that CHIKV infection results in the expansion of epitope-specific CD8$^+$ T cells in the spleen and joint-associated tissues.

Epitope-specific CD8$^+$ T cells display effector functions during CHIKV infection. During chronic virus infection, increased inhibitory receptor expression on antigen-specific CD8$^+$ T cells impairs their functional and proliferative capacity (61, 62). Since CHIKV infection can become persistent, we quantified the expression of the inhibitory receptors PD-1, Tim-3, and Lag-3 on antigen-specific CD8$^+$ T cells during CHIKV(OVA)-AF infection. WT C57BL/6 mice were inoculated with CHIKV(OVA)-AF via s.c. injection in the left rear footpad, and at 10 dpi, the expression of PD-1, Tim-3, and Lag-3 on SIINFEKL-specific CD8$^+$ T cells was quantified. As controls, we included mice inoculated via the intraperitoneal (i.p.) route with 2×10^5 PFU of the lymphocytic choriomeningitis virus Armstrong (LCMV-Arm) strain or mice inoculated via the intravenous (i.v.) route with 2×10^6 PFU of the LCMV clone 13 (LCMV-cl13) strain, in which antigen-specific CD8$^+$ T cells express low or high levels of PD-1, Tim-3, and Lag-3, respectively (61–63). Antigen-specific CD8$^+$ T cells in the spleen of CHIKV(OVA)-AF-infected mice displayed levels of PD-1, Tim-3, and Lag-3 expression comparable to those found in mice infected with the acutely cleared LCMV-Arm strain, and these levels were significantly lower than those detected on antigen-specific CD8$^+$ T cells in mice infected with the chronic LCMV-cl13 strain (Fig. 3A and C). In addition, the expression of these inhibitory receptors was similar on antigen-specific CD8$^+$ T cells present in the joint-associated tissue of mice inoculated s.c. in the foot with CHIKV(OVA)-AF or LCMV-Arm (Fig. 3B and D). Thus, in contrast to LCMV-cl13 infection, antigen-specific CD8$^+$ T cells in CHIKV(OVA)-AF-infected mice did not display a phenotype consistent with functional exhaustion.

We next directly assessed the functionality of epitope-specific CD8$^+$ T cells during CHIKV(OVA)-AF infection. *Ex vivo* stimulation of splenocytes from CHIKV-infected mice

FIG 1 Legend (Continued)
contralateral ankle (D) and in spleen (E) of mock-infected or CHIKV(OVA)-AF-infected mice at 14 dpi. The plots are gated on CD45$^+$ B220$^-$ TCRβ^+ CD8α^+ cells. The numbers embedded in the plots represent the frequency of K^{b}OVA$_{257}$-positive (K^{b}OVA$_{257}^+$) cells within gated CD8$^+$ T cells. (F) Frequency of K^{b}OVA$_{257}^+$ cells among activated CD8$^+$ T cells (CD45$^+$ B220$^-$ TCRβ^+ CD8α^+ CD44^{hi}). (G) Total K^{b}OVA$_{257}^+$ CD8$^+$ T cells (CD45$^+$ B220$^-$ TCRβ^+ CD8α^+ CD44^{hi} K^{b}OVA$_{257}^+$). The data in the graphs represent the mean ± SEM. Data were combined from 2 to 3 independent experiments. Statistically significant differences from the results for mock-infected mice were determined by one-way analysis of variance with Tukey's posttest (for panels A, B, and C and for spleen in panels F and G) or by the Kruskal-Wallis test with Dunn's posttest (for the ipsilateral and contralateral ankles in panels F and G). *, $P < 0.05$; **, $P < 0.01$; ***, $P < 0.001$.

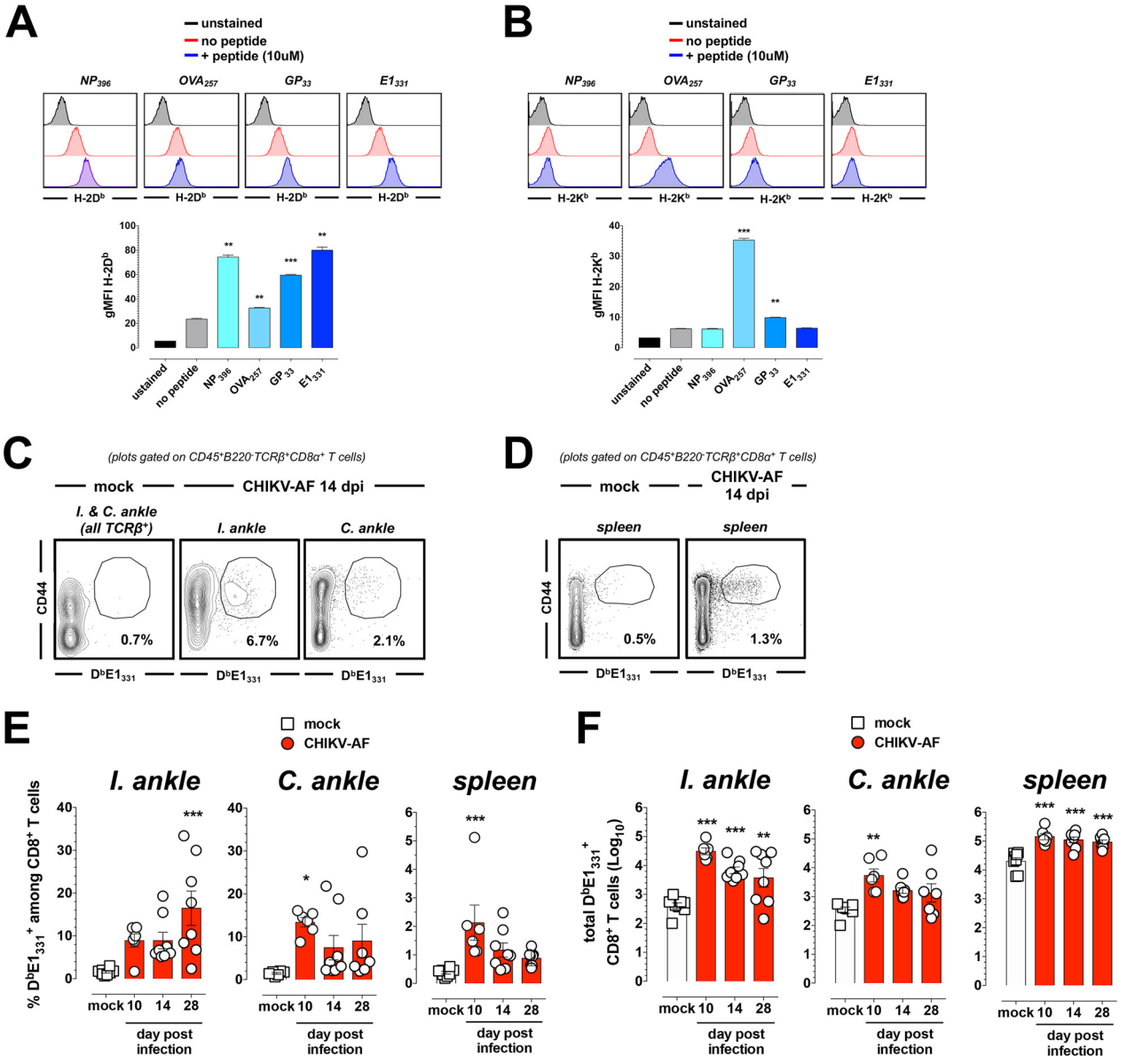

FIG 2 E1-specific CD8$^+$ T cell responses are detected in joint-associated and lymphoid tissue during WT CHIKV-AF infection. (A and B) RMA-S lymphoma cells with stabilized H-2D^b and H-2K^b (incubated overnight at 27°C) were incubated with H-2D^b-restricted (LCMV NP$_{396}$ and LCMV GP$_{33}$), H-2K^b-restricted (OVA$_{257}$ and LCMV GP$_{33}$), or CHIKV E1$_{331}$ peptides for 5 h at 37°C. RMA-S cells in the presence of no peptide were included as a control for destabilization and the loss of MHC class I during culture at 37°C. Stabilization of cell surface MHC class I was visualized by costaining with anti-H-2D^b and H-2K^b antibodies and flow cytometric analysis. (Top) Representative histograms showing the H-2D^b (A) and H-2K^b (B) staining intensity are shown for each peptide (blue) in comparison with that for unstained peptide (gray) and no peptide (red). (Bottom) Graphs represent the geometric mean fluorescence intensity (gMFI) of H-2D^b (A) or H-2K^b (B), showing the mean ± SEM. Data were combined from 2 independent experiments. Statistical differences between each peptide and no peptide were determined by unpaired Student's *t* test. **, $P < 0.01$; ***, $P < 0.001$. (C to F) WT C57BL/6J mice ($n = 6$ to 8 mice/group) were inoculated in the left foot with PBS (mock) or 10^3 PFU of CHIKV-AF. At the indicated dpi, leukocytes were isolated from the ipsilateral (I.) and contralateral (C.) ankles and spleen and CD8$^+$ T cells were quantified by flow cytometry. (C and D) Representative flow cytometry plots showing E1-specific CD8$^+$ T cells in the ipsilateral and contralateral ankles (C) and the spleen (D) of mock- or WT CHIKV-AF-infected mice at 14 dpi. The plots are gated on CD45$^+$ B220$^-$ TCRβ^+ CD8α^+ cells. The numbers embedded in the plots represent the frequency of D^{b}E1$_{331}$-positive (D^{b}E1$_{331}^+$) cells within gated CD8$^+$ T cells. (E) Frequency of D^{b}E1$_{331}^+$ cells among activated CD8$^+$ T cells (CD45$^+$ B220$^-$ TCRβ^+ CD8α^+ CD44^{hi}). (F) Total number of D^{b}E1$_{331}^+$ CD8$^+$ T cells (CD45$^+$ B220$^-$ TCRβ^+ CD8α^+ CD44^{hi} D^{b}E1$_{331}^+$). The data in the graphs represent the mean ± SEM. Data were combined from 2 to 3 independent experiments. Statistically significant differences from the results for mock-infected mice were determined by one-way analysis of variance with Tukey's posttest. *, $P < 0.05$; **, $P < 0.01$; ***, $P < 0.001$.

at 10 dpi with the OVA$_{257}$ or E1$_{331}$ peptide resulted in gamma interferon (IFN-γ) production by ~3% and ~0.5% of CD8$^+$ T cells, respectively (Fig. 4A and B). Time-course analysis revealed that the frequency and total number of IFN-γ-producing (IFN-γ$^+$) CD8$^+$ T cells in the spleen expanded between 5 and 10 dpi (Fig. 4B and C).

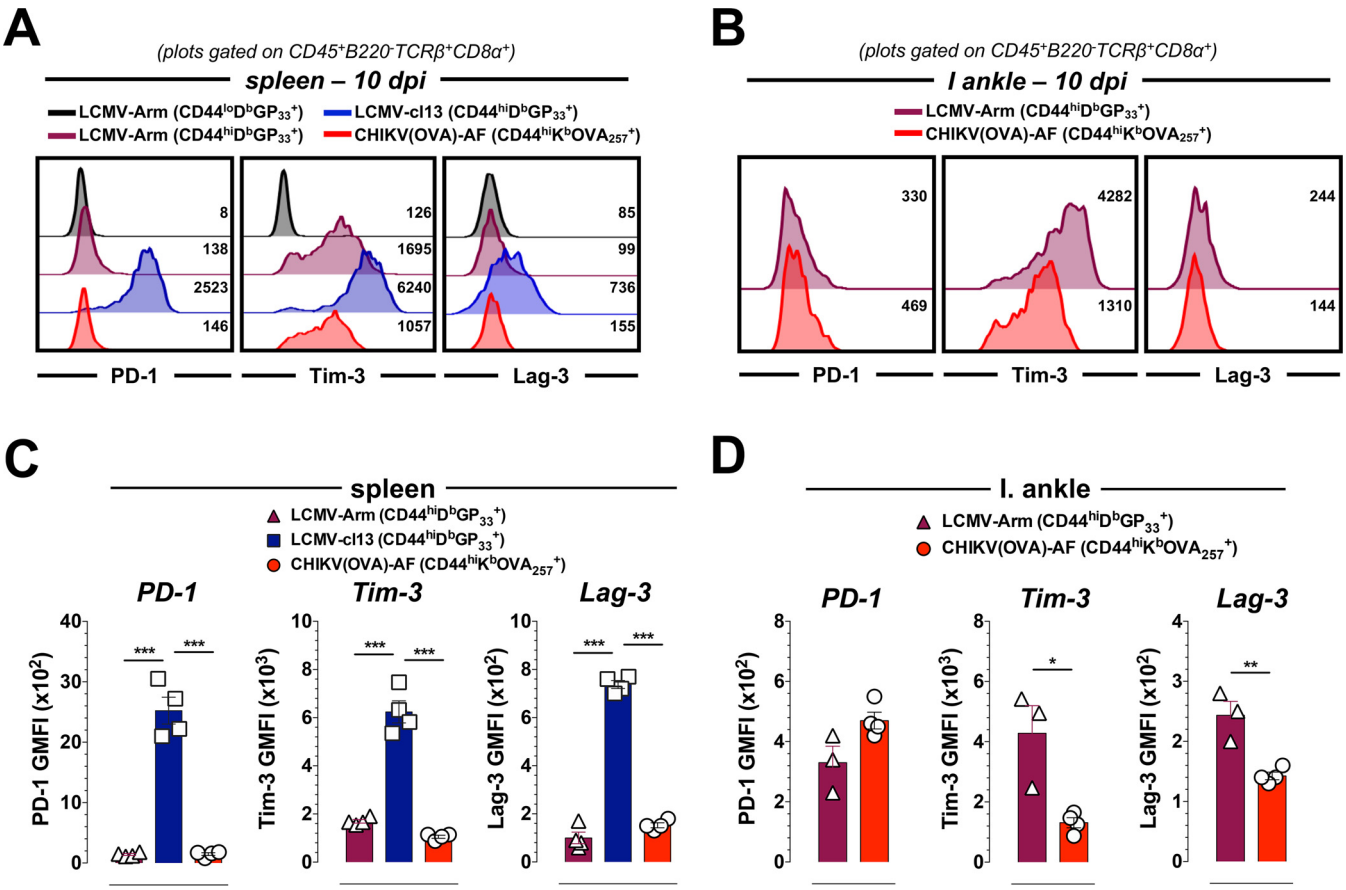

FIG 3 Antigen-specific CD8$^+$ T cells induced in CHIKV(OVA)-AF infection express low levels of the inhibitory receptors PD-1, Tim-3, and Lag-3. (A and C) WT C57BL/6J mice ($n = 4$ mice/group) were inoculated i.p. with 2×10^5 PFU LCMV-Arm, i.v. with 2×10^6 PFU LCMV-cl13, or s.c. in the left foot with 10^3 PFU CHIKV(OVA)-AF. At 10 dpi, PD-1, Tim-3, and Lag-3 expression on antigen-specific CD8$^+$ T cells in the spleen was quantified by flow cytometry. (A) Representative histograms showing PD-1, Tim-3, and Lag-3 expression. PD-1-, Tim-3-, and Lag-3-negative cells are represented by CD45$^+$ B220$^-$ TCRβ^+ CD8α^+ CD44^{lo} tet$^-$ cells from LCMV-Arm-infected mice. The remaining histograms are gated on antigen-specific CD8$^+$ T cells (CD45$^+$ B220$^-$ TCRβ^+ CD8α^+ CD44^{hi} tet$^+$), $D^bGP_{33}{}^+$ cells (LCMV-Arm- and LCMV-cl13-infected mice), or $K^bOVA_{257}{}^+$ cells [CHIKV(OVA)-AF-infected mice]. The numbers embedded in the histograms represent the average geometric mean fluorescence intensity (GMFI) among tetramer-positive cells and are summarized in panel C. (B and D) WT C57BL/6J mice ($n = 3$ to 4 mice/group) were inoculated s.c. in the left foot with 10^3 PFU LCMV-Arm or CHIKV(OVA)-AF. At 10 dpi, PD-1, Tim-3, and Lag-3 expression on antigen-specific CD8$^+$ T cells in the ipsilateral (I.) ankle tissue was assessed by flow cytometry. (B) Representative histograms showing PD-1, Tim-3, and Lag-3 expression on antigen-specific CD8$^+$ T cells. Histograms are gated on antigen-specific CD8$^+$ T cells (CD45$^+$ B220$^-$ TCRβ^+ CD8α^+ CD44^{hi} Tet$^+$), $D^bGP_{33}{}^+$ cells (LCMV-Arm-infected mice), or $K^bOVA_{257}{}^+$ cells [CHIKV(OVA)-AF-infected mice]. The numbers embedded in the histograms represent the average geometric mean fluorescence intensity among tetramer-positive cells and are summarized in panel D. The data in the graphs represent the mean ± SEM. Statistically significant differences were determined by one-way analysis of variance with Tukey's multiple-comparison test (C) or by unpaired Student's t test (D). *, $P < 0.05$; **, $P < 0.01$; ***, $P < 0.001$.

Peptide-stimulated cells also were evaluated for the coproduction of IFN-γ and tumor necrosis factor alpha (TNF-α). We observed an increase in polyfunctional (IFN-γ^+ and TNF-α-producing [TNF-α^+]) CD8$^+$ T cells responding to either OVA_{257} or $E1_{331}$ peptide stimulation between 5 and 10 dpi (Fig. 4D). Polyfunctionality, which was assessed by IFN-γ^+ cells capable of degranulation (i.e., CD107a$^+$), also was increased between 5 and 10 dpi (Fig. 4E) (64, 65).

We separately evaluated the functionality of epitope-specific CD8$^+$ T cells present in joint-associated tissues during CHIKV(OVA)-AF infection. *Ex vivo* stimulation of leukocytes isolated from the ipsilateral ankle at 10 dpi with the OVA_{257} or $E1_{331}$ peptide resulted in IFN-γ production by 13% and 4% of CD8$^+$ T cells, respectively (Fig. 4F and G), resulting in an increased total number of IFN-γ-producing CD8$^+$ T cells at this site (Fig. 4H). Similar responses were detected among CD8$^+$ T cells in the contralateral ankle (Fig. 4F to H). These findings suggest that epitope-specific CD8$^+$ T cells induced during CHIKV(OVA)-AF infection display characteristics of functionally competent effector CD8$^+$ T cells.

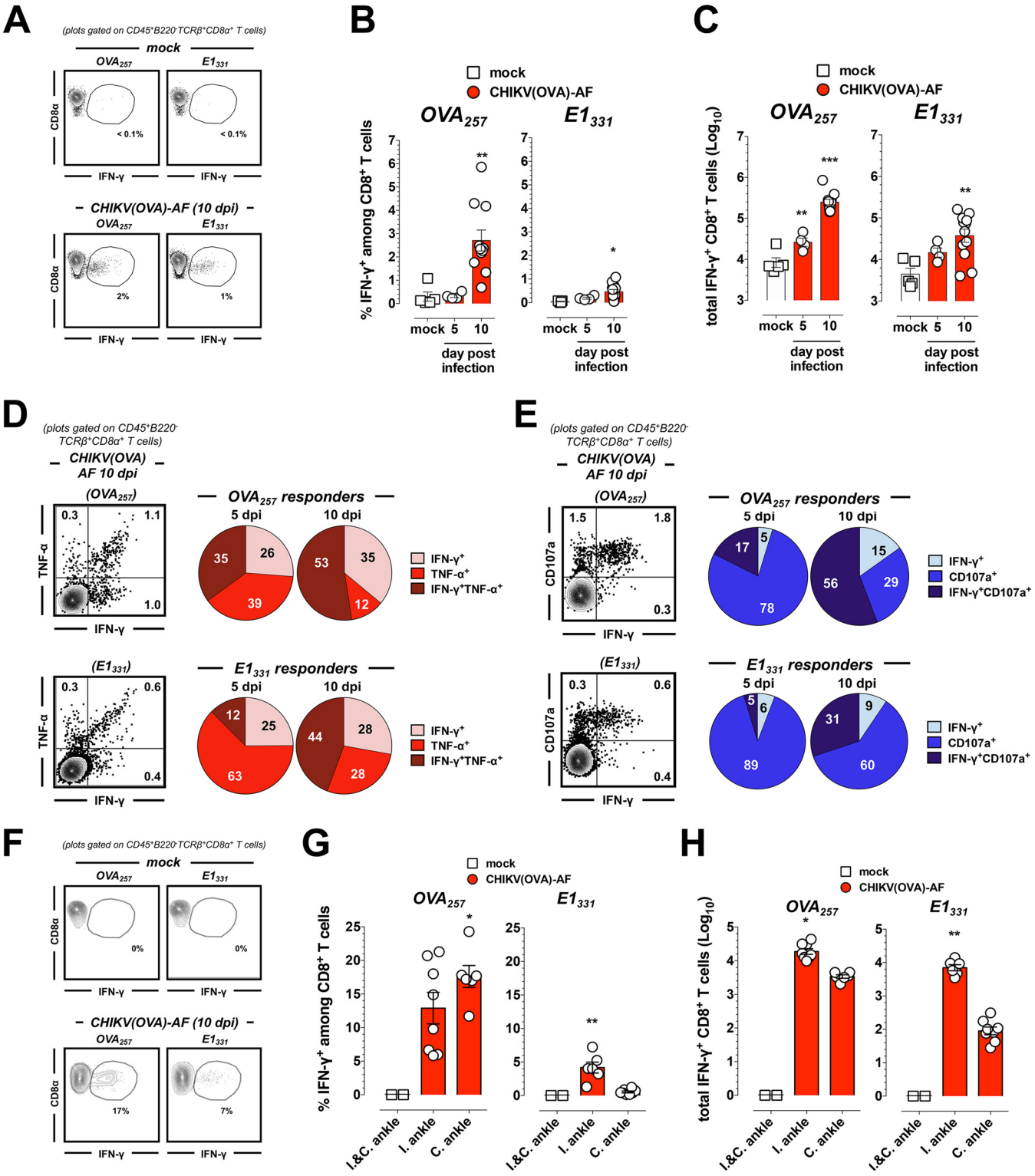

FIG 4 Antigen-specific CD8$^+$ T cells induced during CHIKV(OVA)-AF infection have polyfunctional effector responses. WT C57BL/6J mice ($n = 4$ to 12 mice/group) were inoculated in the left foot with PBS (mock) or 10^3 PFU of CHIKV(OVA)-AF. Spleen cells (5 or 10 dpi) were stimulated with the OVA_{257} or $E1_{331}$ peptide in the presence of anti-CD107a and brefeldin A for 5 h at 37°C. (A) Representative flow cytometry plots showing IFN-γ production in CD8$^+$ T cells following OVA_{257} or $E1_{331}$ peptide stimulation. The plots are gated on CD8$^+$ T cells (CD45$^+$ B220$^-$ TCRβ$^+$ CD8α$^+$). The numbers embedded in the plots represent the frequency of IFN-γ$^+$ cells among gated CD8$^+$ T cells. (B) Frequency of CD8$^+$ T cells (CD45$^+$ B220$^-$ TCRβ$^+$ CD8α$^+$) producing IFN-γ. (C) Total numbers of OVA_{257}- or $E1_{331}$-specific IFN-γ$^+$ CD8$^+$ T cells (CD45$^+$ B220$^-$ TCRβ$^+$ CD8α$^+$ IFN-γ$^+$). (D) Representative dot plots from 10 dpi gated on CD45$^+$ B220$^-$ TCRβ$^+$ CD8α$^+$ T cells. The numbers embedded in the plots represent the frequency among all gated cells. Polyfunctional cytokine-producing responder CD8$^+$ T cells are classified as IFN-γ single positive (IFN-γ$^+$), TNF-α single positive (TNF-α$^+$), or IFN-γ and TNF-α double positive (IFN-γ$^+$ TNF-α$^+$). The pie charts indicate the percentage of each responding population among all responders. (E) Polyfunctional analysis showing the cytokine production and the cytolytic potential

(Continued on next page)

In addition to cytokine production, effector CD8$^+$ T cells mediate antiviral effects by cytolysis of infected cells (66). Given that our *in vitro* peptide stimulation assays suggested that epitope-specific CD8$^+$ T cells in the spleen of CHIKV-infected mice efficiently degranulate (Fig. 4E), we performed *in vivo* cytotoxicity assays to more directly assess their cytolytic capacity (Fig. 5A). To generate target cells, splenocytes from naive mice were loaded with the OVA_{257} peptide or LCMV GP_{33} peptide as a control. To assess the cytolytic capacity of epitope-specific CD8$^+$ T cells in joint-associated tissue or lymphoid tissue, OVA_{257} and GP_{33} peptide-loaded cells were labeled differentially with carboxyfluorescein succinimidyl ester (CFSE), mixed in a 1:1 ratio, and adoptively transferred to the foot (i.e., by s.c. injection) or circulation (i.e., by i.v. injection) of mice that had been inoculated 7 days earlier with CHIKV(OVA)-AF. As controls, the same cell mixtures were transferred into uninfected mice or mice infected with LCMV-Arm. One day after s.c. or i.v. adoptive transfer, single-cell suspensions were generated from the foot or spleen, respectively, and the ratio of OVA_{257}- to GP_{33}-loaded target cells was evaluated by flow cytometry. In naive mice, we detected OVA_{257}- and GP_{33}-loaded target cells in the ankles of mice receiving s.c. adoptive transfer at numbers nearly similar to those in the input (Fig. 5B). As expected, in mice s.c. infected with LCMV-Arm, we detected greatly diminished numbers of GP_{33}-loaded target cells, whereas the OVA_{257}-loaded targets remained intact, validating the specificity of our *in vivo* cytotoxicity assay. In CHIKV(OVA)-AF-infected mice, OVA_{257}-loaded targets were nearly undetectable in the left foot, whereas GP_{33}-loaded target cells were readily detected (Fig. 5B). Similar results were observed in the spleen of infected mice receiving i.v. adoptive transfer of target cells (Fig. 5C). As further validation of our *in vivo* killing assay, mice previously infected via the i.p. route with LCMV-Arm eliminated GP_{33}-pulsed target cells in the spleen (Fig. 5C). Using these data, we calculated the percentage of target cell-specific killing and found that during CHIKV(OVA)-AF infection, CD8$^+$ T cells efficiently eliminated epitope-specific target cells in both joint-associated and lymphoid tissue (Fig. 5D). Thus, the epitope-specific splenic and joint-associated CD8$^+$ T cells induced during CHIKV(OVA)-AF infection are functional effector cells.

Epitope-specific CD8$^+$ T cells are reduced in *Batf3*$^{-/-}$ and *Wdfy4*$^{-/-}$ mice during CHIKV infection. MHC class I-restricted epitopes can be presented by infected cells or by professional antigen-presenting cells (APCs) that acquire exogenous viral antigens, a process termed cross-presentation (67–69). The role of either pathway in CD8$^+$ T cell priming during infection by CHIKV or any alphavirus has not been described. To assess the requirement of cross-presentation for priming antigen-specific CD8$^+$ T cell responses during CHIKV infection, we inoculated WT or *Batf3*$^{-/-}$ mice with CHIKV(OVA)-AF and quantified the antigen-specific CD8$^+$ T cell responses at 10 dpi; the *Batf3*$^{-/-}$ mice are deficient in the DC1 subset of classical dendritic cells (DCs) that cross-present exogenously derived antigens (70–73). The frequency and number of K^bOVA_{257} tet$^+$ CD8$^+$ T cells in the ipsilateral ankle and spleen of *Batf3*$^{-/-}$ mice were reduced but not abolished compared with those in WT mice (Fig. 6A to D). Thus, DC1 cells contribute to, but are not required for, the induction of antigen-specific CD8$^+$ T cell populations during CHIKV infection.

To corroborate the role of cross-presentation in the induction of antigen-specific CD8$^+$ T cell responses during CHIKV infection, we evaluated CD8$^+$ T cell responses in

FIG 4 Legend (Continued)
of responding CD8$^+$ T cells. Dot plots from 10 dpi are gated on CD45$^+$ B220$^-$ TCRβ^+ CD8α^+ T cells, and the numbers embedded in the plots represent the frequency among all gated cells. Responders were classified as IFN-γ^+ single positive (IFN-γ^+), CD107a single positive (CD107a$^+$), or IFN-γ^+ cells that were degranulated (IFN-γ^+ CD107a$^+$) in response to OVA_{257} or $E1_{331}$ peptide stimulation. The pie charts indicate the percentage of each responding population among all responders. (F to H) At 10 dpi, leukocytes were isolated from ipsilateral and contralateral ankle tissue and stimulated with OVA_{257} or $E1_{331}$ peptide in the presence of brefeldin A for 5 h at 37°C. Mock samples represent cells combined from ipsilateral and contralateral tissues. (F) Representative flow plots from ipsilateral ankle tissue showing IFN-γ production by antigen-specific CD8$^+$ T cells in response to OVA_{257} or $E1_{331}$ peptide stimulation. The numbers embedded in the flow plots represent the frequency of CD8$^+$ T cells (CD45$^+$ B220$^-$ TCRβ^+ CD8α^+) producing IFN-γ. (G) Frequency of cells producing IFN-γ among all CD8$^+$ T cells. (H) Total OVA_{257}- and $E1_{331}$-specific IFN-γ^+ CD8$^+$ T cells. The data in the graphs represent the mean ± SEM. Data were combined from 2 to 3 independent experiments. Statistically significant differences between mock- and CHIKV(OVA)-AF-infected mice were determined by one-way analysis of variance with Tukey's posttest (B and C) or by the Kruskal-Wallis test with Dunn's posttest (G and H). *, $P < 0.05$; **, $P < 0.01$; ***, $P < 0.001$.

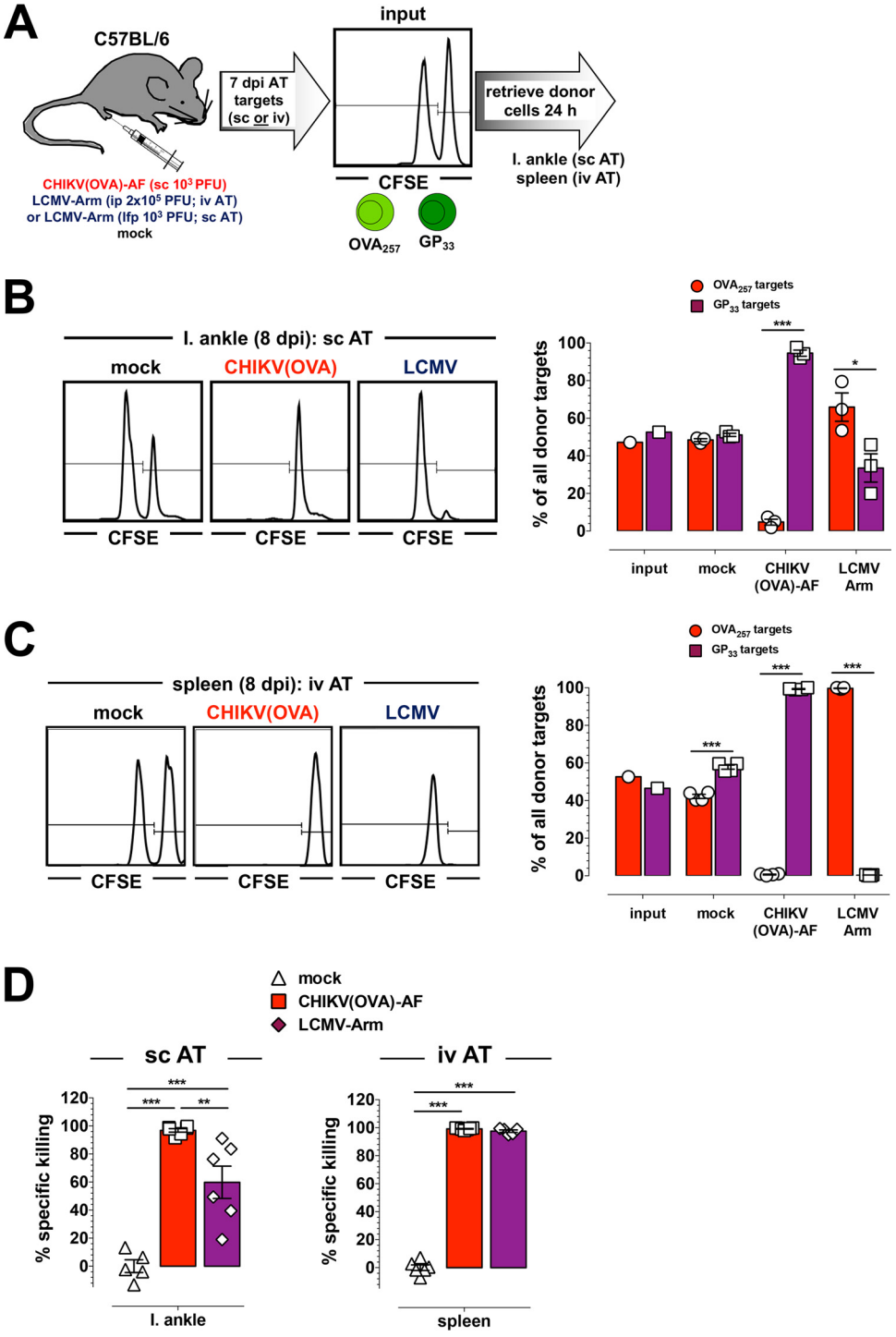

FIG 5 Antigen-specific CD8$^+$ T cells in joint-associated and lymphoid tissue during CHIKV(OVA)-AF infection are cytolytic. (A) WT C57BL6/J mice ($n = 3$ to 6 mice/group) were inoculated s.c. in the left foot with PBS (mock) or 10^3 CHIKV(OVA)-AF. As positive controls, mice were i.p. inoculated with 2×10^6 PFU LCMV-Arm (mice receiving i.v. donor cells) or in the left foot s.c. with 10^3 PFU LCMV-Arm (mice receiving donor cells via the s.c. route in the foot). At 7 dpi, naive splenic donor cells were pulsed with OVA_{257} or GP_{33} peptide, differentially labeled with CFSE (OVA_{257} CFSE^{lo}, GP_{33} CFSE^{hi}), mixed together at a 1:1 ratio (input), and transferred adoptively. At 24 h post-adoptive transfer, donor cells were retrieved from the ipsilateral (I.) ankle or from the spleen, and the ratio of OVA_{257}- to GP_{33}-loaded targets was determined. (B) (Left) Representative histograms showing donor target cells retrieved from the ipsilateral ankle following footpad s.c. adoptive transfer. Histograms are gated on total donor CFSE-positive (CFSE$^+$) cells; (right) frequency of OVA_{257} or GP_{33} target populations among total donor cells (CFSE$^+$ cells) in the ipsilateral ankle. (C) (Left) Representative histograms showing donor cells retrieved from the spleen following i.v. adoptive transfer; (right) frequency of OVA_{257} or GP_{33} target populations among total donor cells (CFSE$^+$ cells) in the spleen.

(Continued on next page)

CHIKV(OVA)-AF-infected *Wdfy4*$^{-/-}$ mice; these mice have normal numbers of DC1 cells but lack the intracellular mechanisms required to cross-present antigen (74). At 10 dpi, the frequency and total cell numbers of K^bOVA_{257} tet$^+$ CD8$^+$ T cells in the ipsilateral and contralateral ankles and the spleen of CHIKV-infected *Wdfy4*$^{-/-}$ mice were reduced compared with those in CHIKV-infected WT mice (Fig. 6E and F). Together, these findings indicate that both antigen cross-presentation by DC1 cells and possibly other myeloid cells and direct presentation by infected cells drive the CHIKV-specific CD8$^+$ T cell response.

The CHIKV burden in tissues is unaffected by CD8$^+$ T cells. To evaluate the impact of CD8$^+$ T cells on the course of CHIKV infection, we compared the viral burden in joint-associated tissues and the spleen of WT and CD8$\alpha^{-/-}$ mice infected with CHIKV-AF at 7, 14, 28, and 42 dpi (Fig. 7). Remarkably, no differences in viral infection were observed in the ipsilateral ankle (Fig. 7A), contralateral ankle (Fig. 7B), or spleen (Fig. 7C) of WT and CD8$\alpha^{-/-}$ mice at any of the time points examined. Thus, despite eliciting effector CD8$^+$ T cell responses in both joint-associated tissues and the spleen, the absence of these cells had no demonstrable antiviral impact on CHIKV infection in tissues.

The lack of CD8$^+$ T cell antiviral effects in joint-associated tissues is specific to CHIKV infection. To determine if the lack of CD8$^+$ T cell-mediated antiviral effects in joint-associated tissues was unique to CHIKV infection, we assessed the control of LCMV-Arm, which produces an acute infection that resolves in a CD8$^+$ T cell-dependent manner (75, 76). We adapted the LCMV infection model that is based on i.p. inoculation of 6- to 8-week-old WT C57BL/6 mice with 2×10^5 PFU of LCMV-Arm (77); however, in our experiments, similar to the CHIKV studies, we inoculated 4-week-old WT C57BL6 mice to determine if LCMV-Arm is efficiently cleared in young mice. For comparison, we also inoculated via the i.v. route 4-week-old WT C57BL/6 mice with 2×10^6 PFU of LCMV-cl13, which establishes a chronic infection (48). Mice inoculated i.v. with LCMV-cl13 displayed weight loss from 5 to 8 dpi (Fig. 8A), which was associated with a high viral burden at 10 dpi in the serum, spleen, liver, and kidney (Fig. 8B). In contrast, mice inoculated via the i.p. route with LCMV-Arm showed weight gain throughout the duration of the experiment, and infectious virus was undetectable in serum, spleen, liver, and kidney at 10 dpi (Fig. 8A and B). These data with LCMV-Arm and LCMV-cl13 in 4-week-old WT C57BL/6 mice are consistent with published results utilizing 6- to 8-week-old mice (48, 78, 79).

To assess if CD8$^+$ T cells are required for the clearance of LCMV administered via s.c. injection in the foot, we inoculated WT and CD8$\alpha^{-/-}$ C57BL/6 mice with 10^3 PFU of either LCMV-Arm or LCMV-cl13 s.c. in the left foot, the dose and route used in our CHIKV experiments. At 10 dpi, high levels of infectious virus were present in the ipsilateral ankle and spleen of LCMV-Arm-infected CD8$\alpha^{-/-}$ mice but not those of WT mice (Fig. 8C). Similar results were observed when we measured the LCMV-Arm viral burden in tissue via reverse transcription (RT)-quantitative PCR (qPCR); viral RNA levels were higher in the ipsilateral ankle and spleen of CD8$\alpha^{-/-}$ mice than in those of WT mice (Fig. 8D). Thus, in contrast to the findings obtained after CHIKV infection, CD8$^+$ T cells have an antiviral effect in joint-associated and lymphoid tissues of mice inoculated with a similar dose of LCMV-Arm by a similar route. Since LCMV-Arm infection is cleared by CD8$^+$ T cells (75, 76), we also tested whether CD8$^+$ T cells had an antiviral role in joint-associated and lymphoid tissues following s.c. inoculation of LCMV-cl13. As shown in Fig. 8E, viral RNA levels in the ipsilateral ankle and spleen of LCMV-cl13-infected

FIG 5 Legend (Continued)
(D) The specific killing of OVA_{257}-loaded targets in CHIKV(OVA)-AF-infected mice or GP_{33}-loaded targets in LCMV-Arm-infected mice was calculated as described in Materials and Methods. The data in the graphs represent the mean ± SEM. Data were combined from 2 to 3 independent experiments. Statistically significant differences in the specific killing of target cells in mock-infected mice infected with CHIKV(OVA)-AF or LCMV-Arm were determined by unpaired Student's *t* test (B and C) or by one-way analysis of variance with Tukey's posttest (D). *, $P < 0.05$; **, $P < 0.01$; ***, $P < 0.001$.

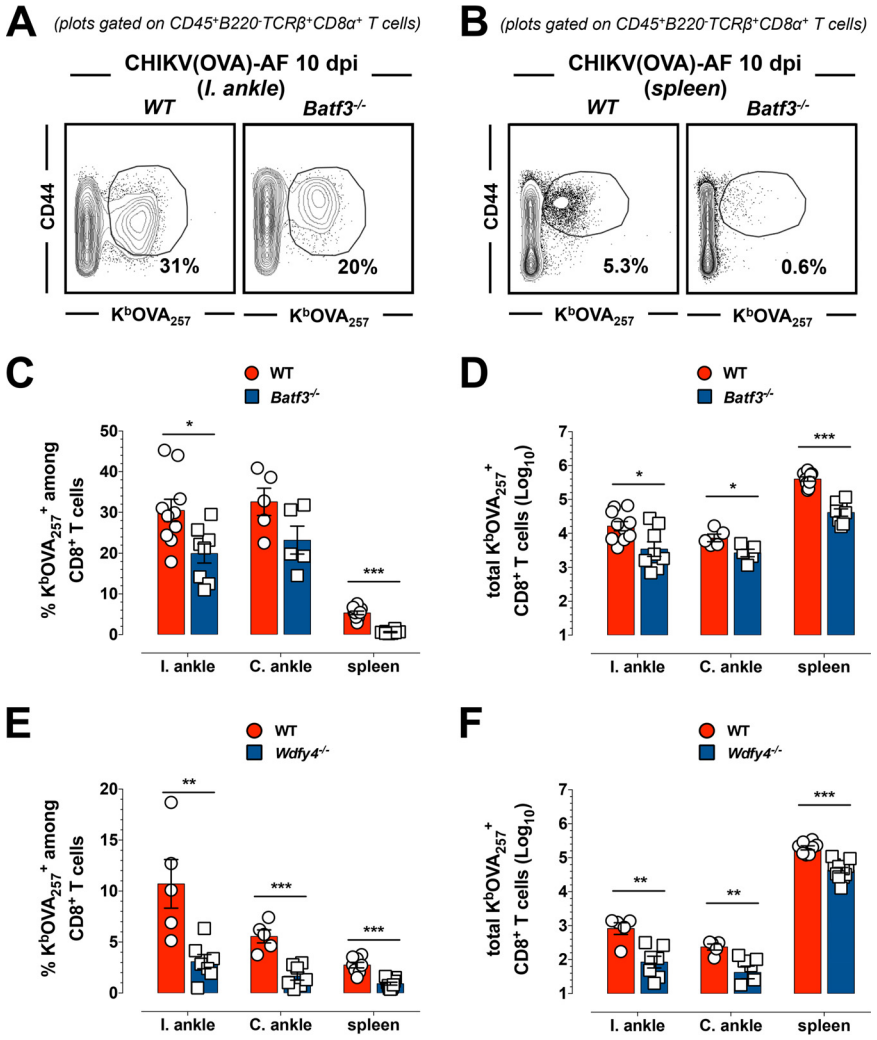

FIG 6 Disruption of *Batf3* and *Wdfy4* reduces the induction of antigen-specific CD8$^+$ T cells during CHIKV(OVA)-AF infection. (A to D) WT C57BL6/J mice ($n = 5$ to 10 mice/group) and congenic *Batf3*$^{-/-}$ mice ($n = 5$ to 8 mice/group) were inoculated in the left foot with 10^3 PFU of CHIKV(OVA)-AF. At 10 dpi, antigen-specific CD8$^+$ T cells (CD45$^+$ B220$^-$ TCRβ^+ CD8α^+ CD44^{hi} K^{b}OVA$_{257}^+$) were enumerated in the ipsilateral (I.) and contralateral (C.) ankle and the spleen. Representative flow cytometry plots showing K^{b}OVA$_{257}^+$ CD8$^+$ T cells at 10 dpi from the ipsilateral ankle (A) and the spleen (B) of WT and *Batf3*$^{-/-}$ mice. The plots are gated on CD8$^+$ T cells (CD45$^+$ B220$^-$ TCRβ^+ CD8α^+). The numbers embedded in the plots represent the frequency of K^{b}OVA$_{257}^+$ cells among CD8$^+$ T cells. (C) Frequency of K^{b}OVA$_{257}^+$ cells among CD8$^+$ T cells (CD45$^+$ B220$^-$ TCRβ^+ CD8α^+ CD44^{hi}). (D) Total numbers of K^{b}OVA$_{257}^+$ CD8$^+$ T cells (CD45$^+$ B220$^-$ TCRβ^+ CD8α^+ CD44^{hi} K^{b}OVA$_{257}^+$). (E and F) WT C57BL6/J mice ($n = 5$ to 8 mice/group) and congenic *Wdfy4*$^{-/-}$ mice ($n = 7$ to 11 mice/group) were inoculated in the left foot with 10^3 PFU of CHIKV(OVA)-AF. (E) Frequency of K^{b}OVA$_{257}^+$ cells among CD8$^+$ T cells (CD45$^+$ CD3$^+$ CD8α^+). (F) Total K^{b}OVA$_{257}^+$ CD8$^+$ T cells (CD45$^+$ CD3$^+$ CD8α^+ K^{b}OVA$_{257}^+$). The data in the graphs represent the mean ± SEM. Data were combined from 2 to 3 independent experiments. Statistically significant differences between WT and *Batf3*$^{-/-}$ mice or WT and *Wdfy4*$^{-/-}$ mice were determined by unpaired Student's *t* test. *, $P < 0.05$; **, $P < 0.01$; ***, $P < 0.001$.

CD8$\alpha^{-/-}$ mice were increased compared with the levels in the same tissues of WT mice, suggesting that CD8$^+$ T cells also exert an antiviral effect against LCMV-cl13 infection in joint-associated and lymphoid tissues. Thus, the lack of a demonstrable effect of the complete absence of CD8$^+$ T cells on CHIKV infection in joint-associated and splenic tissues is independent of mouse age, the virus inoculation route, and the tissues analyzed. Rather, the data suggest that CHIKV evades CD8$^+$ T cell immune surveillance.

Preexisting effector antigen-specific CD8$^+$ T cells enhance CHIKV clearance. To test whether the presence of preexisting effector CD8$^+$ T cells could enhance the clearance of CHIKV infection, we adoptively transferred activated OT-I transgene-

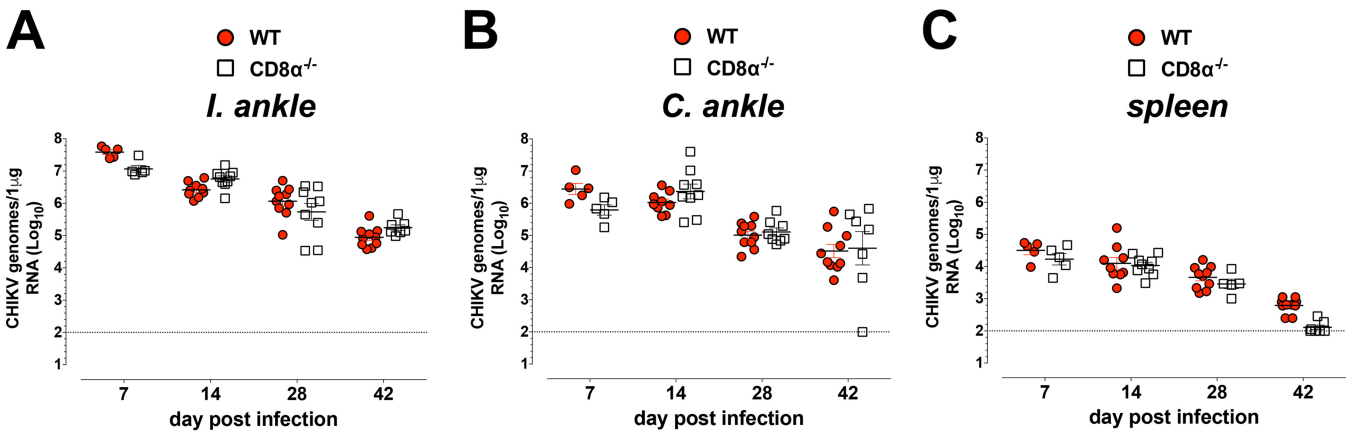

FIG 7 The viral burdens in joint-associated and lymphoid tissue are similar in CHIKV-infected WT and CD8$\alpha^{-/-}$ mice. WT C57BL/6J mice ($n = 5$ to 10 mice/time point) or congenic C57BL/6J CD8$\alpha^{-/-}$ mice ($n = 5$ to 9 mice per time point) were inoculated in the left foot with 10^3 PFU of CHIKV-AF. (A to C) On the indicated days postinfection, CHIKV RNA in the ipsilateral (I.) ankle (A), contralateral (C.) ankle (B), and spleen (C) was quantified by RT-qPCR. The data in the graphs represent the mean ± SEM. Data were combined from 4 independent experiments. No statistically significance differences between WT and CD8$\alpha^{-/-}$ mice were detected by two-way analysis of variance.

positive (Tg$^+$) CD8$^+$ T effector cells into naive mice prior to inoculation with either CHIKV(OVA)-AF or CHIKV(OVA4K)-AF, which encodes a single N-to-K amino acid substitution in the SIINFEKL epitope that abrogates the stimulation of OT-I Tg$^+$ CD8$^+$ T cells (Fig. 9A) (80). Following *in vitro* activation and expansion, OT-I Tg$^+$ CD8$^+$ T cells exhibited an activated phenotype, as shown by elevated CD25 and CD69 expression compared with that by naive CD8$^+$ T cells (Fig. 9B). Following peptide stimulation, activated OT-I Tg$^+$ CD8$^+$ T cells produced cytokines (IFN-γ and TNF-α) and exhibited the capacity to degranulate (Fig. 9C). Next, 10^7 activated OT-I Tg$^+$ CD8$^+$ T cells or naive splenocytes as a control were adoptively transferred into WT mice. Two hours later, mice were inoculated s.c. with 10^3 PFU of either CHIKV(OVA)-AF or CHIKV(OVA4K)-AF. At 7 dpi, more than 50% of the circulating CD8$^+$ T cells in mice inoculated with CHIKV(OVA)-AF were OT-I Tg$^+$ CD8$^+$ T cells (Fig. 9D). In comparison, the frequency of OT-I Tg$^+$ CD8$^+$ T cells was reduced 4- to 5-fold in mice inoculated with CHIKV(OVA4K)-AF (Fig. 9D); thus, OT-I Tg$^+$ CD8$^+$ T cells are preferentially expanded and maintained in mice inoculated with CHIKV(OVA)-AF encoding an intact SIINFEKL epitope. At 28 dpi, the viral burden was reduced in the ipsilateral ankle (3-fold) and the contralateral ankle (6-fold) of CHIKV(OVA)-AF-infected mice that received OT-I Tg$^+$ CD8$^+$ T cells compared with the burden in mice that received naive splenocytes (Fig. 9E and F). In the spleen, the CHIKV burden was decreased 16-fold in CHIKV(OVA)-AF-infected mice that received OT-I Tg$^+$ CD8$^+$ T cells compared with that in mice that received naive splenocytes (Fig. 9G). The adoptive transfer of OT-I Tg$^+$ CD8$^+$ T cells had no effect on the viral burden in mice infected with CHIKV(OVA4K)-AF (Fig. 9E to G), indicating that the antiviral effects of the donor cells are epitope specific. Thus, the presence of preexisting antigen-specific CD8$^+$ T cells prior to CHIKV infection can promote CHIKV clearance, but this effect is more potent in the spleen than in joint-associated tissues.

We next tested if the activation and expansion of antigen-specific effector CD8$^+$ T cells *in vivo* prior to CHIKV infection could enhance the clearance of CHIKV infection. WT mice were vaccinated with whole OVA antigen or no antigen (control) in the presence of an adjuvant composed of agonistic anti-CD40 and the Toll-like receptor 3 agonist poly(I·C), which induces robust OVA-specific T cell responses in mice (81). At 7 days postvaccination (dpv), mice were inoculated with CHIKV(OVA)-AF, and the viral burden was measured in joint-associated tissue and spleen at 28 dpi (35 dpv) (Fig. 10A). Induction of SIINFEKL-specific CD8$^+$ T cells by this immunization was confirmed by increases in both the frequency and the number of K^bOVA_{257} tet$^+$ CD8$^+$ T cells in the spleen of mice at 7 dpv (Fig. 10B and C). Moreover, *ex vivo* stimulation of splenocytes

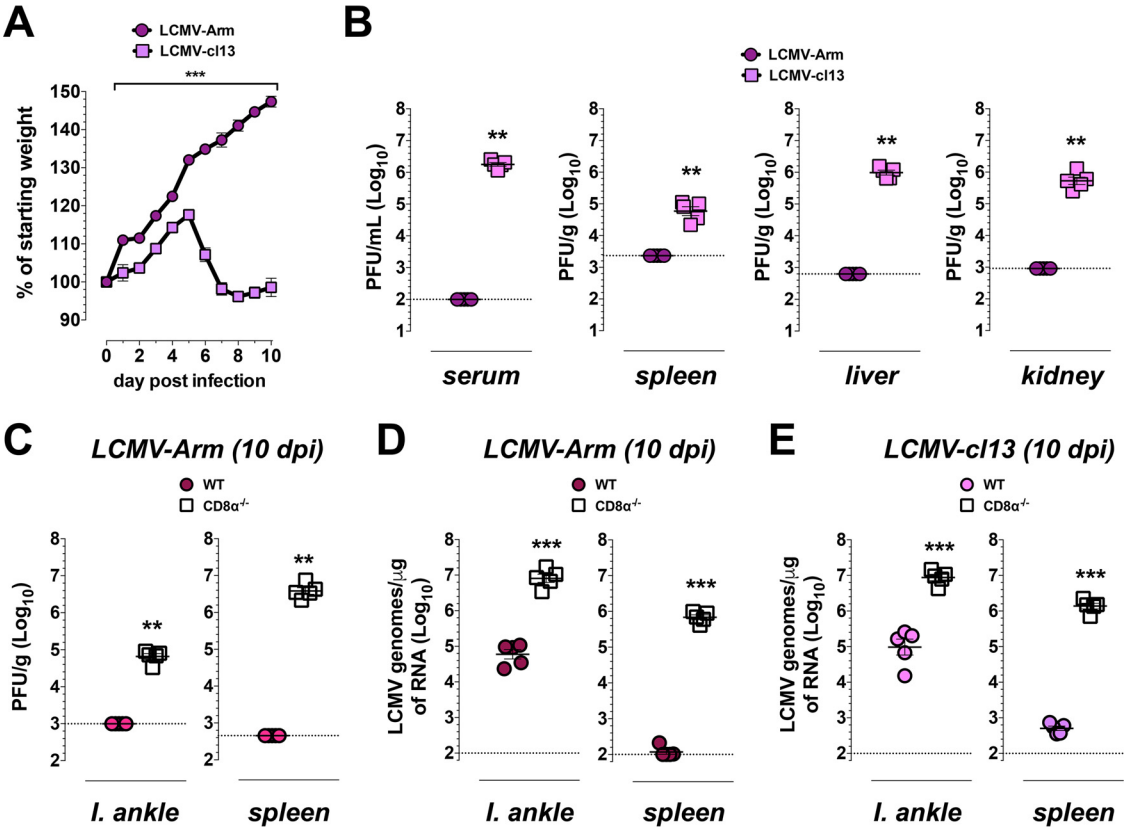

FIG 8 The absence of CD8$^+$ T cells impairs the clearance of LCMV in joint-associated and lymphoid tissue. (A and B) WT C57BL/6J mice were inoculated with 2×10^5 PFU LCMV-Arm via the i.p. route ($n = 5$ mice) or 2×10^6 PFU LCMV-cl13 via the i.v. route ($n = 5$ mice). (A) Weight gain was monitored daily and is reported as a percentage of the starting weight. (B) At 10 dpi, viral loads in the serum, spleen, liver, and kidney were quantified by plaque assay. Bars represent the SEM. Statistically significant differences were determined by two-way analysis of variance with Bonferroni's posttest (A) or by Mann-Whitney test (B). **, $P < 0.01$; ***, $P < 0.001$. (C) WT ($n = 5$) or CD8$\alpha^{-/-}$ ($n = 5$) C57BL/6J mice were inoculated in the left foot with 10^3 PFU of LCMV-Arm. At 10 dpi, viral titers in the ipsilateral (I.) ankle and spleen were determined by plaque assay. (D and E) WT ($n = 5$) or CD8$\alpha^{-/-}$ ($n = 5$) C57BL/6J mice were inoculated in the left foot with 10^3 PFU of LCMV-Arm (D) or LCMV-cl13 (E). At 10 dpi, LCMV RNA in the ipsilateral ankle and spleen was quantified by RT-qPCR. The data in the graphs represent the mean ± SEM. Data were combined from 2 independent experiments. Statistically significant differences were determined by the Mann-Whitney test (C) or unpaired Student's *t* test (D and E). **, $P < 0.01$; ***, $P < 0.001$.

from control mice and mice immunized with the OVA_{257} peptide also demonstrated that immunization increased the frequency and number of IFN-γ-producing CD8$^+$ T cells (Fig. 10D to F). In addition, a large fraction of these cells coproduced IFN-γ and TNF-α or IFN-γ and CD107a (Fig. 10E and F), indicating that the immunization elicited SIINFEKL-specific, polyfunctional, effector CD8$^+$ T cells.

At 28 dpi, the viral burden was quantified in the contralateral ankle and spleen of mice treated with phosphate-buffered saline (PBS), treated with adjuvant alone [anti-CD40/poly(I·C)], or vaccinated with OVA plus anti-CD40/poly(I·C) (Fig. 10G and H). Despite the presence of preexisting SIINFEKL-specific effector CD8$^+$ T cells, there was no decrease in viral infection in the joint-associated tissues of vaccinated mice (Fig. 10G). In contrast, viral infection was reduced in the spleen of mice vaccinated with adjuvanted OVA compared with that in the spleen of mice treated with PBS or adjuvant alone (Fig. 10H). Thus, a T cell-based vaccine that elicits effector CD8$^+$ T cells has antiviral effects in an antigen-specific manner in the spleen but not in the joint-associated tissue of CHIKV-infected mice.

DISCUSSION

Infection with CHIKV is associated with the persistence of virus in lymphoid and joint-associated tissue that is not cleared by adaptive immune responses. CD8$^+$ T cells are critical for the control and clearance of viral infections, but their role during CHIKV

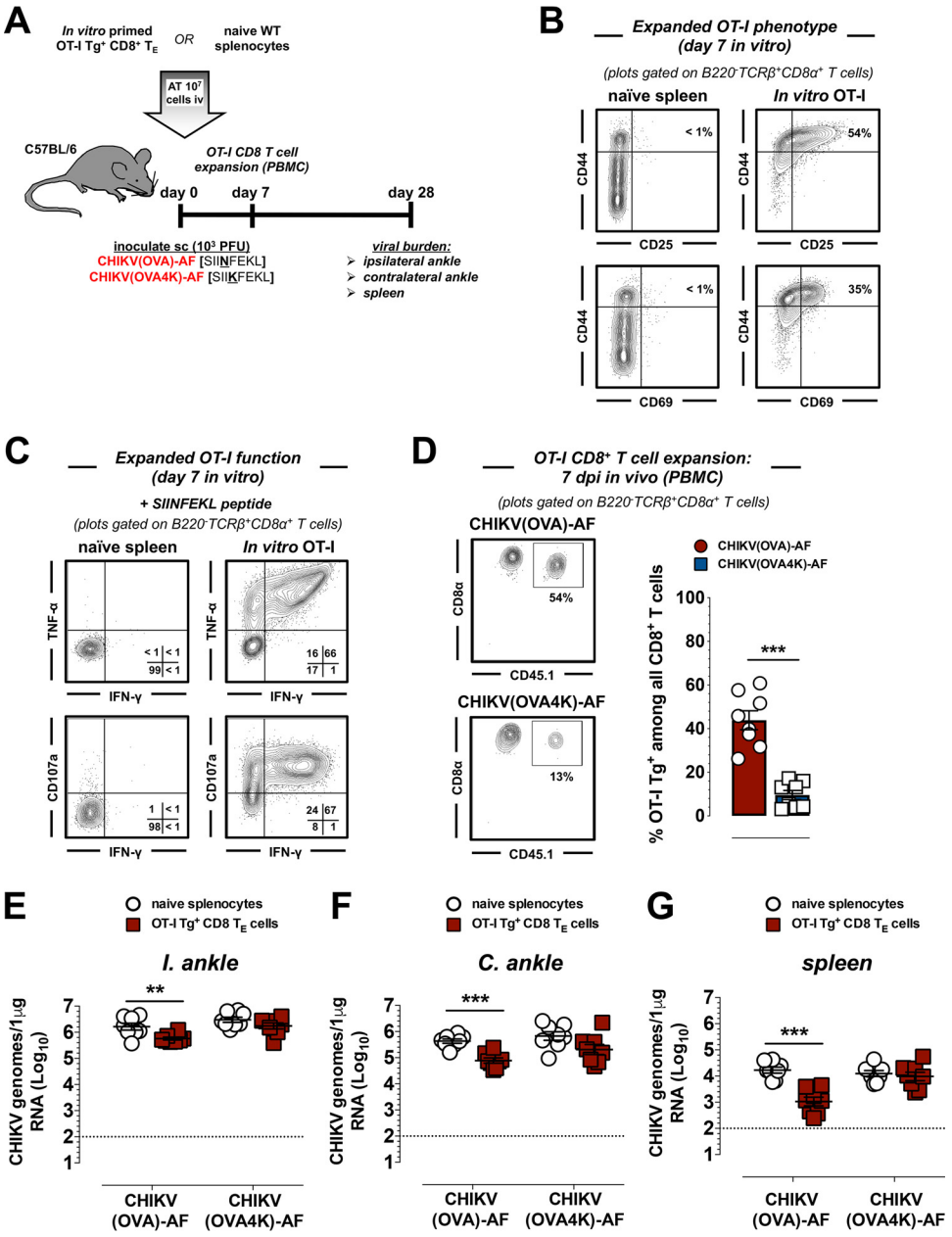

FIG 9 Adoptive transfer of OT-I Tg$^+$ CD8$^+$ T effector cells prior to CHIKV infection enhances viral clearance. (A) Schematic of experimental design. (B and C) *In vitro*-expanded OT-I Tg$^+$ CD8$^+$ T cells were analyzed for expression of CD25 and CD69 activation markers (B) and function (cytokine production and degranulation) (C) in response to SIINFEKL peptide stimulation. (D to G) Activated OT-I Tg$^+$ CD8$^+$ T cells or naive splenocytes (10^7) were adoptively transferred i.v. into recipient mice. Two hours later, the mice were inoculated in the left foot with 10^3 PFU of CHIKV(OVA)-AF or CHIKV(OVA4K)-AF. (D) At 7 dpi, OT-I Tg$^+$ CD8$^+$ T cells were quantified in the peripheral blood. (Left) Representative dot plots show endogenous CD8$^+$ T cells (CD45.1$^-$) and donor OT-I Tg$^+$ CD8$^+$ T cells (CD45.1$^+$) within the total CD8$^+$ T cell compartment. The numbers embedded in the plots represent the frequency of OT-I Tg$^+$ CD8$^+$ T cells among total CD8$^+$ T cells. (Right) The frequency of OT-I Tg$^+$ CD8$^+$ T cells among all CD8$^+$ T cells is summarized in the graph. (E to G) At 28 dpi, CHIKV RNA in the ipsilateral (I.) and contralateral (C.) ankle and the spleen was quantified by RT-qPCR. The data in the graphs represent the mean ± SEM. Data were derived from 2 independent experiment. Statistical significance in panels D to G was determined by an unpaired Student's *t* tests. **, $P < 0.01$; ***, $P < 0.001$. PBMC, peripheral blood mononuclear cells; T_E cells, effector T cells.

infection is not well-defined. Using a recombinant CHIKV strain encoding a CD8$^+$ TCR epitope from ovalbumin and an E1 peptide-specific MHC class I tetramer, we found that antigen-specific CD8$^+$ T cells expand in lymphoid and joint-associated tissue following CHIKV infection and that this expansion is reduced in *Batf3*$^{-/-}$ and *Wdfy4*$^{-/-}$ mice

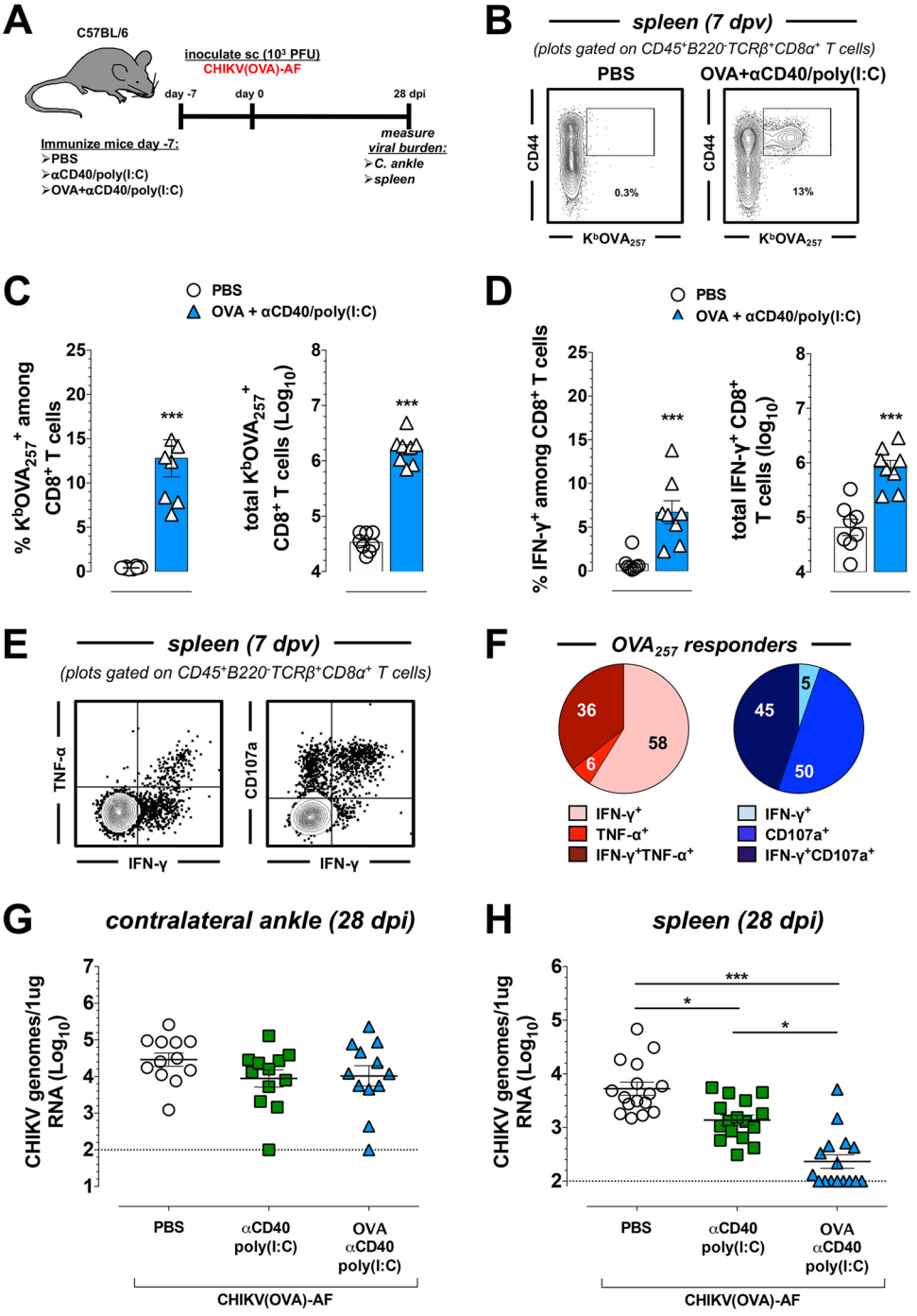

FIG 10 Prophylactic vaccination with a T cell-based vaccine accelerates CHIKV clearance from the spleen but not joint-associated tissue. (A) Schematic of experimental design. WT C57BL/6 mice were immunized with PBS ($n = 16$), anti-CD40/poly(I·C) ($n = 16$), or OVA and anti-CD40/poly(I·C) ($n = 16$) 7 days prior to (day −7) CHIKV infection. At 7 days postvaccination (dpv), mice were inoculated in the left foot with 10^3 PFU CHIKV(OVA)-AF. (B) Representative flow plots showing $K^bOVA_{257}{}^+$ $CD8^+$ T cells in the spleen of mice immunized with PBS or OVA and anti-CD40/poly(I·C) at 7 dpv. (C and D) The frequency and total number of $K^bOVA_{257}{}^+$ cells among $CD8^+$ T cells ($CD45^+$ $B220^-$ $TCR\beta^+$ $CD8\alpha^+$ $CD44^{hi}$ $K^bOVA_{257}{}^+$) (C) and the frequency and total number of OVA_{257}-specific IFN-γ^+ $CD8^+$ T cells ($CD45^+$ $B220^-$ $TCR\beta^+$ $CD8\alpha^+$ IFN-γ^+) (D) following 5 h of *in vitro* stimulation with OVA_{257} peptide in mice immunized with PBS or OVA and anti-CD40/poly(I·C) at 7 dpv ($n = 8$ mice per group). (E) Representative dot plots of splenocytes from 7 dpv gated on $CD45^+$ $B220^-$ $TCR\beta^+$ $CD8\alpha^+$ T cells showing responder cells by either IFN-γ and TNF-α or by IFN-γ and CD107a. (F) Polyfunctional cytokine-producing responder $CD8^+$ T cells are classified as IFN-γ single positive (IFN-γ^+), TNF-α single positive (TNF-α^+), or IFN-γ and TNF-α double positive (IFN-γ^+ TNF-α^+) in response to OVA_{257} peptide stimulation. Alternatively, responders were classified as IFN-γ^+ single positive (IFN-γ^+), CD107a single positive ($CD107a^+$), or IFN-γ^+ cells that were degranulated (IFN-γ^+ $CD107a^+$) in response to OVA_{257} peptide stimulation. The pie charts indicate the percentage of each responding population among all

(Continued on next page)

defective for antigen cross-presentation. Moreover, *ex vivo* and *in vivo* analyses revealed that epitope-specific splenic and joint-associated CD8$^+$ T cells induced during CHIKV infection display characteristics of functional effector CD8$^+$ T cells, including cytokine production and cytolytic activity. Nevertheless, experiments in WT and CD8$\alpha^{-/-}$ mice showed that, unlike LCMV infection, CHIKV infection in lymphoid and joint-associated tissues is unaffected by CD8$^+$ T cells. Finally, we found that the presence of preexisting effector antigen-specific CD8$^+$ T cells can accelerate CHIKV clearance from lymphoid tissue but not joint-associated tissue. These data suggest that CHIKV establishes and maintains a persistent infection in joint-associated tissue by evading CD8$^+$ T cell immunity.

Antigen-specific CD8$^+$ T cell responses are induced during CHIKV infection. The control of CHIKV infection depends on adaptive immune responses (32–34, 39, 82); however, the contribution of CD8$^+$ T cells has remained poorly understood. Activated CD8$^+$ T cells are elevated in the circulation of CHIKV-infected patients (22, 30, 40, 41), and studies in NHPs and mice have demonstrated that CD8$^+$ T cells expand in the circulation, lymphoid tissue, and joint-associated tissue following CHIKV infection (38, 39, 42, 43, 82, 83). In addition, a number of distinct vaccine candidates elicit CHIKV-specific CD8$^+$ T cell responses, but their role in protective immunity has rarely been evaluated (60, 84–89). In one study in mice, vaccine-elicited T cells were poorly protective against CHIKV infection (84). More recently, a study used cytomegalovirus- and adenovirus-vectored vaccines encoding CHIKV fusion peptides capable of eliciting CD4$^+$ and CD8$^+$ T cell responses to investigate the antiviral activity of T cells during CHIKV infection (51). This study found that prime-boost vaccination prior to intramuscular CHIKV injection reduced the viral burden in muscle tissue in a CD8$^+$ T cell-dependent manner. However, the viral burden in joint-associated tissue was unaffected in immunized mice (51).

Our data show that antigen-experienced (CD44^{hi}), epitope-specific CD8$^+$ T cells accumulate in spleen and joint-associated tissues of CHIKV-infected mice. These responses peaked at 10 to 14 dpi; however, CD44^{hi} antigen-specific CD8$^+$ T cells remained detectable during the chronic phase of infection, particularly in joint-associated tissues. These findings are similar to those of prior studies reporting the presence of CHIKV-specific CD4$^+$ T cells in joint-associated tissues of mice at ~90 dpi (82). The role of CHIKV-specific T cell populations that persist in joint-associated tissues in both protection and pathology requires further investigation. Collectively, these data suggest that CHIKV infection results in the priming and expansion of antigen-specific CD8$^+$ T cells that accumulate in the spleen and joint-associated tissues.

Cytokine production and cytolytic activity by antigen-specific CD8$^+$ T cells are important antiviral effector functions. In some cases, such as persistent virus infection or immunosuppressive environments, these effector functions can become compromised (90). However, we found that antigen-specific CD8$^+$ T cells in CHIKV-infected mice displayed lower levels of Lag-3, PD-1, and Tim-3 inhibitory receptors than antigen-specific CD8$^+$ T cells in LCMV-cl13-infected mice, suggesting that the cells are not functionally exhausted. Consistent with these data, we found that antigen-specific CD8$^+$ T cells in the spleen of CHIKV-infected mice exhibit polyfunctionality by producing multiple proinflammatory cytokines (IFN-γ and TNF-α) and degranulating (i.e., showing cytolytic potential) upon peptide restimulation. Thus, the classical effector functions of CD8$^+$ T cells are not compromised during CHIKV infection, at least when analyzed *ex vivo*. These results are consistent with those of studies demonstrating that circulating CHIKV-specific CD8$^+$ T cells in patients with acute and chronic CHIKV disease also produce proinflammatory cytokines and exhibit cytolytic potential in response to

FIG 10 Legend (Continued)
responders. Statistical significance in panels C and D was determined by unpaired Student's *t* test. ***, $P < 0.001$. (G and H) At 28 dpi (35 dpv), CHIKV RNA in the contralateral (C.) ankle and the spleen was quantified by RT-qPCR. Data were combined from 3 independent experiments. Statistical significance was determined by the Kruskal-Wallis test with Dunn's posttest. *, $P < 0.05$; ***, $P < 0.001$.

ex vivo peptide restimulation (41, 91). Similar observations were made using CD8$^+$ T cells from CHIKV-infected NHPs; however, as discussed above, the magnitude and breadth of the CHIKV-specific CD8$^+$ T cell responses are diminished in aged NHPs that develop persistent CHIKV infection (39). *In vivo* cytotoxicity is a hallmark of antigen-specific CD8$^+$ T cells induced during acute viral infection and correlates with protection against many virus infections (92–95). We found that both the joint-associated and splenic antigen-specific CD8$^+$ T cells induced during CHIKV infection are cytolytic against peptide-loaded splenocytes *in vivo*, suggesting that CD8$^+$ T cells have the potential to control CHIKV infection via specific lysis of antigen-bearing target cells. Collectively, these data indicate that the epitope-specific splenic and joint-associated CD8$^+$ T cells induced during CHIKV infection have features of functionally competent effector cells that should promote the control of infection.

Antigen-specific CD8$^+$ T cell priming during CHIKV infection. The mechanisms by which infection with CHIKV or other alphaviruses prime CD8$^+$ T cell responses have not been elucidated. In general, APCs prime CD8$^+$ T cells by proteolytically processing endogenously synthesized (i.e., direct presentation) or exogenously acquired (i.e., cross-presentation) antigens to peptides that bind to MHC class I molecules (96). To identify the cells and the pathways involved in priming CHIKV-specific CD8$^+$ T cell responses, we analyzed these responses in *Batf3*$^{-/-}$ mice selectively deficient in DC1 cells, the primary DC subset that cross-presents antigen to CD8$^+$ T cells in mice (70). Since other DC1 effector functions are impacted by the absence of these cells in *Batf3*$^{-/-}$ mice, we also evaluated CHIKV-specific CD8$^+$ T cell responses in mice lacking WDFY4, which is essential for the cross-presentation of antigens (74). Importantly, *Wdfy4*$^{-/-}$ DC1 cells express normal levels of MHC class I at steady state and after activation and can directly present antigen. In both CHIKV-infected *Batf3*$^{-/-}$ and *Wdfy4*$^{-/-}$ mice, epitope-specific CD8$^+$ T cell responses were reduced in magnitude, particularly in the spleen, suggesting that antigen cross-presentation by DC1 and possibly other cells contributes to the priming of epitope-specific effector CD8$^+$ T cells during CHIKV infection. However, epitope-specific CD8$^+$ T cell responses were not eliminated in CHIKV-infected *Batf3*$^{-/-}$ or *Wdfy4*$^{-/-}$ mice, suggesting that other antigen presentation mechanisms contribute to the generation and expansion of epitope-specific effector CD8$^+$ T cells during CHIKV infection.

The CHIKV burden in joint-associated tissue is unaffected by the absence of CD8$^+$ T cells or the presence of preexisting, activated effector CD8$^+$ T cells. Despite the priming and expansion of effector CD8$^+$ T cells during CHIKV infection, their accumulation in spleen and joint-associated tissues, and their apparently intact effector functions, we found that the viral burden at these sites was equivalent in WT and CD8$\alpha^{-/-}$ mice, which lack CD8$^+$ T cells and certain subsets of dendritic cells (97, 98), during both the acute and the chronic phases of infection. These findings are consistent with those of other studies which reported indistinguishable viremia in CHIKV-infected WT and CD8$\alpha^{-/-}$ mice and WT mice depleted of CD8$^+$ T cells (82), further suggesting that CD8$^+$ T cells have remarkably little or no effect on the control of CHIKV infection. The mechanism(s) by which CHIKV infection evades control by CD8$^+$ T cells remains to be elucidated. In this study, we found that the antiviral activity of CD8$^+$ T cells is required for the control of LCMV-Arm and LCMV-cl13 infection in the spleen and joint-associated tissue following inoculation of mice via the same route with a similar dose of virus, indicating that the lack of antiviral activity of CD8$^+$ T cells during CHIKV infection is not due to the age of the mouse, the route of inoculation, or the specific tissues evaluated. Although endogenously primed CD8$^+$ T cell responses appear to be ineffective at controlling CHIKV infection, we found that the adoptive transfer of antigen-specific CD8$^+$ T effector cells prior to CHIKV infection led to modest viral clearance in joint-associated tissue and more robust clearance in lymphoid tissue. Moreover, using a T cell-dependent immunization approach, we found that the expansion of antigen-specific effector CD8$^+$ T cells *in vivo* prior to virus inoculation enhanced the clearance of CHIKV infection in the spleen but not in joint-associated tissues. Together, these data suggest that preexisting antigen-specific CD8$^+$ T cells elicit a more

pronounced antiviral effect in lymphoid tissue than in joint-associated tissue. These findings are similar to those of studies of RRV infection in mice, which found that CD8$^+$ T cells contributed to the control of RRV infection in some tissues but failed to mediate an antiviral effect in joint-associated tissues (44). Thus, our findings provide a foundation for investigating the mechanisms by which CHIKV and other arthritogenic alphaviruses evade the CD8$^+$ T cell response in joint-associated tissues. This deficit could be due to impaired antigen presentation by CHIKV-infected cells, such as dermal fibroblasts and skeletal muscle cells, which harbor persistent CHIKV infection (36); spatial relationships between antigen-specific CD8$^+$ T cells and CHIKV-infected cells that limit CD8$^+$ T cell killing; immunosuppressive microenvironments; or the acquisition of escape mutations in dominant CD8$^+$ TCR epitopes.

MATERIALS AND METHODS

Ethics statement. This study was conducted in accordance with the recommendations in the *Guide for the Care and Use of Laboratory Animals* (99) and the American Veterinary Medical Association (AVMA) *Guidelines for the Euthanasia of Animals* (100). All animal experiments conducted at the University of Colorado Anschutz Medical Campus were performed with the approval of the Institutional Animal Care and Use Committee (IACUC) at the University of Colorado School of Medicine (assurance number A3269-01) under protocols 00026 and 00215. Animal experiments conducted at Washington University were approved by the IACUC at the Washington University School of Medicine (assurance number A3381-01).

Cells. BHK-21 cells (ATCC CCL10) were grown in α-minimal essential medium (Life Technologies) supplemented with 10% bovine calf serum (HyClone), 10% tryptose phosphate broth, penicillin, streptomycin, and 0.29 mg/ml L-glutamine. Vero cells (ATCC CCL81) were grown in Dulbecco's modified Eagle medium (DMEM)–F-12 medium (Life Technologies) supplemented with 10% fetal bovine serum (FBS; Lonza), nonessential amino acids (Life Technologies), sodium bicarbonate, penicillin, streptomycin, and 0.29 mg/ml L-glutamine.

Viruses. CHIKV AF15561 (CHIKV-AF) and the recombinant CHIKV-AF strain encoding immunodominant CD8 (SIINFEKL) and CD4 (ISQAVHAAHAEINEAGR) [CHIKV(OVA)-AF] T cell epitopes for ovalbumin have been described previously (46). CHIKV(OVA)-AF with a single N-to-K amino acid substitution at position 4 of the SIINFEKL epitope (SIIKFEKL) [CHIKV(OVA4K)-AF] was generated by site-directed mutagenesis. The substitution of K for N at position 4 of the SIINFEKL epitope preserves peptide binding to H-2K^b yet greatly diminishes the stimulation of CD8$^+$ T cells (80). Virus stocks were generated by electroporation of BHK-21 cells with viral RNA transcribed *in vitro* from plasmid DNA templates as described previously (46, 101). LCMV-Arm (clone 53b) and LCMV-cl13 stocks were propagated by a single passage in BHK-21 cells. CHIKV infectious titers were determined by plaque assay on BHK-21 cells, and LCMV titers were determined by plaque assay on Vero cells (42, 102). All work with infectious LCMV was conducted under biosafety level 2 conditions, and work with infectious CHIKV was conducted under biosafety level 3 conditions.

Mouse experiments. WT C57BL/6J mice (catalog number 000664), congenic CD8$\alpha^{-/-}$ mice (B6.129S2-*Cd8a*^{tm1Mak}/J; catalog number 002665), congenic CD45.1$^+$ OT-I Tg$^+$ mice expressing the TCR specific for the ovalbumin-derived H-2K^b-rescrited immunodominant CD8$^+$ TCR epitope SIINFEKL [C57BL/6-Tg(TcraTcrb)1100Mjb/J; catalog number 003831], *Batf3*$^{-/-}$ mice [B6.129S(C)-*Batf3*^{tm1Kmm}/J; catalog number 013755], and *Wdfy4*$^{-/-}$ mice (C57BL/6NJ-*Wdfy4*$^{em1(IMPC)J}$/J; catalog number 029334) mice were acquired from The Jackson Laboratory and/or bred in specific-pathogen-free facilities at the University of Colorado Anschutz Medical Campus or Washington University. For virus inoculation, 4-week-old male and female mice were injected subcutaneously in the left rear footpad with 10^3 PFU of CHIKV or LCMV in a 10-μl volume. For standard LCMV infections, mice were inoculated with 2×10^5 PFU of LCMV-Arm via the i.p. route or with 2×10^6 PFU of LCMV-cl13 via the i.v. route. For immunization studies, mice were injected i.p. with 50 μg of polyinosinic-poly(C) [poly(I·C); catalog number P1530; Sigma] and 50 μg of anti-mouse CD40 antibody (clone FGK4.5; catalog number BE0016-2; BioXcell) with or without 0.5 mg of ovalbumin (vac-pova-25; Invivogen). Mice were euthanized by sedation with isoflurane vapors followed by bilateral thoracotomy. Blood was collected, and mice were perfused by intracardiac injection of 10 ml of PBS. PBS-perfused tissues were removed and homogenized in the TRIzol reagent (Life Technologies) for RNA isolation or PBS–1% FBS for tissue homogenate using a MagNA Lyser instrument (Roche).

Tissue processing for flow cytometry. Single-cell suspensions of splenocytes were generated by dispersion through 100-μm-mesh-size nylon mesh cell strainers. Ankle tissues were incubated with glass beads in digestion buffer (RPMI supplemented with 10% FBS, 2.5 mg/ml collagenase type I [Worthington Biochemical], and 1.7 mg/ml DNase I [Roche]) with vigorous shaking at 37°C for 1.5 h. Following digestion, the cells were filtered through a 100-μm-mesh-size nylon mesh cell strainer. Erythrocytes were lysed by incubation with ammonium-chloride-potassium (ACK) red blood cell lysis buffer (spleen and ankle tissue). Total viable cell numbers were enumerated by trypan blue exclusion.

Identification of CHIKV E1$_{331}$ MHC class I restriction and generation of CHIKV E1$_{331}$-specific MHC class I tetramer. The C57BL/6 mouse-derived RMA-S lymphoma cell line, which is deficient in TAP2, was used in an MHC class I stabilization assay (52). Briefly, RMA-S cells were cultured overnight at 27°C to promote the accumulation of peptide-absent MHC class I H-2D^b and H-2K^b molecules at the cell

surface. RMA-S cells harboring empty H-2D^b and H-2K^b were coincubated with immunodominant CD8$^+$ T cell peptides at 10 μM for 5 h at 37°C. The peptides used were $OVA_{257–264}$ (SIINFEKL; H-2K^b restricted), LCMV $NP_{396–404}$ (FQPQNGQFI; H-2D^b restricted), LCMV $GP_{33–41}$ (KAVYNFATC; H-2D^b and H-2K^b restricted), and CHIKV $E1_{331–339}$ (HSMTNAVTI; restriction unknown). LCMV and CHIKV peptides were acquired from GenScript, and the OVA peptide was purchased from Invivogen. Next, peptide-mediated MHC class I stabilization was quantified by staining RMA-S cells with anti-mouse H-2D^b (clone 28-14-8) and H-2K^b (clone AF6-14-8) antibodies while on ice. Cells were fixed in 1% paraformaldehyde (PFA) for 15 min, and MHC class I stabilization was quantified by flow cytometry. H-2D^b$E1_{331}$ MHC class I tetramers were generated by the NIH Tetramer Core Facility at Emory University.

***Ex vivo* peptide stimulation, degranulation assay, and cell staining procedures.** Single-cell suspensions from spleen or ankle tissue were stimulated *ex vivo* with the OVA_{257} peptide (SIINFEKL) or the CHIKV CD8$^+$ T cell immunodominant epitope $E1_{331}$ peptide (HSMTNAVTI) at 1 μM in the presence of 3 μg/ml of brefeldin A and 0.5 μg/ml of anti-mouse CD107a (catalog number 1D4B; BioLegend) for 5 h at 37°C (46, 50, 64). Following stimulation, the cells were incubated with a fixable live/dead cell stain (catalog number L34955; Invitrogen) and then incubated with anti-mouse Fcγ receptor III (FcγRIII)/FcγRII (93) for 20 min on ice in PBS supplemented with 1% FBS and 15 mM NaN_3 (fluorescence-activated cells sorting [FACS] buffer). The cells were then stained with fluorophore-conjugated antibodies against TCRβ (catalog number H57-597; BioLegend), B220 (catalog number RA3-6B2; BD Biosciences), CD8α (catalog number 53-6.7; BioLegend), and CD45 (catalog number 30-F11; BioLegend) to delineate the CD8$^+$ T cells. Following surface staining, the cells were fixed and permeabilized in a paraformaldehyde-saponin buffer (4% PFA plus 1 mg/ml saponin and 1 mM HEPES, pH 7.3, in PBS) for 15 min at room temperature. The cells were washed two times in saponin buffer (1 mg/ml saponin in FACS buffer) following fixation. For intracellular cytokine staining, permeabilized cells were incubated with anti-IFN-γ (catalog number XMG1.2; BioLegend) and anti-TNF-α (catalog number MP6-XT22; BioLegend) antibodies in saponin buffer for 45 min at room temperature. Following intracellular staining, the cells were washed three times in saponin buffer.

To identify antigen-specific CD8$^+$ T cells using MHC class I tetramers, cells were stained with a live/dead fixable viability dye and anti-mouse FcγRIII/FcγRII as described above. The cells were then costained with K^bOVA_{257} or K^b$E1_{331}$ tetramers in the presence of anti-mouse CD8α (catalog number 53-6.7; BioLegend) for 30 min at 37°C. The following remaining surface antibodies were added and the mixture was incubated for an additional 20 min at 37°C: anti-mouse TCRβ (clone H57-597; BioLegend), CD3ε (clone 145-2C11; BioLegend), B220 (clone RA3-6B2; BD Biosciences), CD44 (clone IM7; BioLegend), CD45 (clone 30-F11; BioLegend), PD-1 (clone RMP1-30; BioLegend), Tim-3 (clone 5D12/Tim-3; BD Biosciences), and Lag-3 (clone C9B7W; BD Biosciences). Subsequently, the cells were washed with PBS three times and fixed in PBS containing 1% PFA for 15 min at room temperature. Samples were processed on a BD Fortessa X-20 or a BD FACSCalibur flow cytometer.

***In vivo* cytotoxicity assay.** Antigen-specific CD8$^+$ T cell cytotoxicity was quantified using an *in vivo* assay adapted from published protocols (94, 103, 104). WT C57BL/6 mice were inoculated with 10^3 PFU of CHIKV(OVA)-AF or 10^3 PFU of LCMV-Arm via s.c. inoculation in the foot or 2×10^5 PFU of LCMV-Arm via i.p. injection. Target cells were prepared from naive WT C57BL/6 spleen cells by pulsing with either OVA_{257} or GP_{33} at 1 μg/ml for 1 h at 37°C. Target cells were washed three times with PBS, differentially labeled with CFSE (OVA_{257} at 0.25 μM, GP_{33} at 2.5 μM) for 10 min at 37°C, washed three times in RPMI plus 10% FBS, and then mixed together at a ratio of 1:1 (OVA_{257}/GP_{33}). Mixing of the differentially labeled cells was confirmed by flow cytometry prior to adoptive transfer. Target cells were adoptively transferred i.v. (3×10^6 to 6×10^6 total cells, 1.5×10^6 to 3×10^6 cells of each target population) into mice inoculated with CHIKV(OVA)-AF or LCMV-Arm (at 7 dpi). In some experiments, the target cells were adoptively transferred via s.c. injection in the foot. At 24 h post-adoptive transfer, donor cells were retrieved from the spleen of mice receiving target cells through i.v. transfer or from the left ankle of mice receiving target cells through s.c. transfer, and the ratio of OVA_{257} to GP_{33} donor target cells was quantified by flow cytometry. Specific lysis of target cells was determined using the calculation [1 – (ratio of infected cells/ratio of mock-infected cells)] $\times$ 100, where the ratio is the quotient of target pulsed donor cells to control pulsed donor cells.

Expansion of OT-I Tg$^+$ CD8$^+$ T effector cells and adoptive transfer. Splenocytes from OT-I Tg$^+$ CD45.1 congenic mice were cocultured with OVA_{257}-pulsed splenocytes from naive WT mice (1 μg OVA_{257} peptide per 10^6 cells incubated at 37°C for 1 h) in RPMI plus 10% FBS supplemented with 50 μM β-mercaptoethanol (βME). After 2 days of coculture, fresh RPMI plus 10% FBS and βME containing 10 U/ml recombinant mouse interleukin-2 (catalog number 212-12; PeproTech) was added. After 7 days, expanded OT-I Tg$^+$ CD8$^+$ T cells were enriched from the debris and apoptotic cells by purification over the Lympholyte-M reagent (catalog number CL5031; Cedarlane). Purified cells were confirmed to be OT-I Tg$^+$ CD8$^+$ T cells by flow cytometry and adoptively transferred i.v. (10^7 cells per mouse) 2 h prior to virus inoculation. As a control, 10^7 naive splenocytes were adoptively transferred i.v. to mice.

Quantification of viral RNA by RT-qPCR. For both CHIKV and LCMV RNA quantification assays, tissue samples were homogenized in the TRIzol reagent (catalog number 15596018; Life Technologies) and RNA was isolated using an Ambion PureLink RNA minikit (catalog number 12183025; Life Technologies). During RNA isolation, samples were subjected to an on-column DNase (catalog number 12185010; Life Technologies) digestion to eliminate DNA contamination. cDNA was generated using random primers and SuperScript IV reverse transcriptase (catalog number 18091050; Life Technologies).

Quantification of CHIKV genomes was performed as previously described (33, 105). Briefly, qPCR was performed with CHIKV-specific forward (5′-TTTGCGTGCCACTCTGG-3′) and reverse (5′-CGGGTCACCACA AAGTACAA-3′) primers and an internal TaqMan probe (5′-ACTTGCTTTGATCGCCTTGGTGAGA-3′). The

total number of CHIKV genomes was extrapolated from a standard curve generated from samples containing 10^8 to 10^0 copies of CHIKV genomic RNA spiked into RNA from BHK-21 cells, and cDNA was synthesized *in vitro* under conditions identical to those for samples from tissues. Mock-infected tissues and no-template reverse transcription reactions were included in each assay to ensure RT-qPCR specificity.

For quantification of LCMV RNA, we utilized a previously described assay with minor modifications (106). Following the generation of cDNA as described above, qPCR was performed using LCMV glycoprotein-specific forward (5′-CATTCACCTGGACTTTGTCA-3′) and reverse (5′-GCAACTGCTGTGTTCCC GAAAC-3′) primers with an internal TaqMan probe (5′-TCCAGGTGGTTATTGCCTGACCAA-3′). An LCMV-specific standard curve was generated as described above using RNA transcribed *in vitro* from a plasmid containing the full-length LCMV glycoprotein sequence (pHCMV/LCMV-Arm53b; catalog number 15796; AddGene). All qPCRs were performed using an Applied Biosystems QuantStudio (version 7) or ViiA (version 7) analyzer.

Data analysis. All data processing, graphical representations, and statistical analyses were conducted using GraphPad Prism (version 8.2) software. Graphical representations of all data are expressed as the mean $\pm$ the standard error of the mean (SEM), and statistical significance was determined using the tests indicated in the figure legends. Variances in data were deemed significant with a P value of <0.05.

ACKNOWLEDGMENTS

This research was supported by Public Health Service grants R01 AI108725 (to T.E.M.) and R01 AI141436 (to T.E.M. and M.S.D.) from the National Institute of Allergy and Infectious Diseases. B.J.D. was supported by grant T32 AR007534.

We thank the NIH Tetramer Core Facility, Emory University, Atlanta, GA, for providing CHIKV D^bE1_{331} MHC class I tetramers.

The funders had no role in study design, data collection and interpretation, or the decision to submit the work for publication.

M.S.D. is a consultant for Inbios and Atreca and is on the Scientific Advisory Board of Moderna.

REFERENCES

1. Suhrbier A, Jaffar-Bandjee M-C, Gasque P. 2012. Arthritogenic alphaviruses—an overview. Nat Rev Rheumatol 8:420–429. https://doi.org/10.1038/nrrheum.2012.64.
2. Robinson MC. 1955. An epidemic of virus disease in Southern Province, Tanganyika Territory, in 1952–1953. I. Clinical features. Trans R Soc Trop Med Hyg 49:28–32. https://doi.org/10.1016/0035-9203(55)90080-8.
3. Gear J, Reid FP. 1957. The occurrence of a dengue-like fever in the North-Eastern Transvaal. I. Clinical features and isolation of virus. South Afr Med J Suid-Afr Tydskr Vir Geneeskd 31:253–257.
4. Ross RW. 1956. The Newala epidemic. III. The virus: isolation, pathogenic properties and relationship to the epidemic. J Hyg (Lond) 54:177–191. https://doi.org/10.1017/s0022172400044442.
5. Carey DE, Myers RM, DeRanitz CM, Jadhav M, Reuben R. 1969. The 1964 chikungunya epidemic at Vellore, South India, including observations on concurrent dengue. Trans R Soc Trop Med Hyg 63:434–445. https://doi.org/10.1016/0035-9203(69)90030-3.
6. Shah KV, Gibbs CJ, Banerjee G. 1964. Virological investigation of the epidemic of haemorrhagic fever in Calcutta: isolation of three strains of chikungunya virus. Indian J Med Res 52:676–683.
7. Myers RM, Carey DE, Reuben R, Jesudass ES, De Ranitz C, Jadhav M. 1965. The 1964 epidemic of dengue-like fever in South India: isolation of chikungunya virus from human sera and from mosquitoes. Indian J Med Res 53:694–701.
8. Sergon K, Yahaya AA, Brown J, Bedja SA, Mlindasse M, Agata N, Allaranger Y, Ball MD, Powers AM, Ofula V, Onyango C, Konongoi LS, Sang R, Njenga MK, Breiman RF. 2007. Seroprevalence of chikungunya virus infection on Grande Comore Island, Union of the Comoros, 2005. Am J Trop Med Hyg 76:1189–1193. https://doi.org/10.4269/ajtmh.2007.76.1189.
9. Powers AM, Logue CH. 2007. Changing patterns of chikungunya virus: re-emergence of a zoonotic arbovirus. J Gen Virol 88:2363–2377. https://doi.org/10.1099/vir.0.82858-0.
10. Sissoko D, Malvy D, Giry C, Delmas G, Paquet C, Gabrie P, Pettinelli F, Sanquer MA, Pierre V. 2008. Outbreak of chikungunya fever in Mayotte, Comoros Archipelago, 2005–2006. Trans R Soc Trop Med Hyg 102:780–786. https://doi.org/10.1016/j.trstmh.2008.02.018.
11. Moro ML, Gagliotti C, Silvi G, Angelini R, Sambri V, Rezza G, Massimiliani E, Mattivi A, Grilli E, Finarelli AC, Spataro N, Pierro AM, Seyler T, Macini P, Chikungunya Study Group. 2010. Chikungunya virus in north-eastern Italy: a seroprevalence survey. Am J Trop Med Hyg 82:508–511. https://doi.org/10.4269/ajtmh.2010.09-0322.
12. Grandadam M, Caro V, Plumet S, Thiberge J-M, Souarès Y, Failloux A-B, Tolou HJ, Budelot M, Cosserat D, Leparc-Goffart I, Desprès P. 2011. Chikungunya virus, southeastern France. Emerg Infect Dis 17:910–913. https://doi.org/10.3201/eid1705.101873.
13. Leparc-Goffart I, Nougairede A, Cassadou S, Prat C, de Lamballerie X. 2014. Chikungunya in the Americas. Lancet 383:514. https://doi.org/10.1016/S0140-6736(14)60185-9.
14. Zeller H, Van Bortel W, Sudre B. 2016. Chikungunya: its history in Africa and Asia and its spread to new regions in 2013–2014. J Infect Dis 214:S436–S440. https://doi.org/10.1093/infdis/jiw391.
15. Burt FJ, Chen W, Miner JJ, Lenschow DJ, Merits A, Schnettler E, Kohl A, Rudd PA, Taylor A, Herrero LJ, Zaid S, Ng LFP, Mahalingham S. 2017. Chikungunya virus: an update on the biology and pathogenesis of this emerging pathogen. Lancet Infect Dis 17:e107–e117. https://doi.org/10.1016/S1473-3099(16)30385-1.
16. Borgherini G, Poubeau P, Staikowsky F, Lory M, Moullec NL, Becquart JP, Wengling C, Michault A, Paganin F. 2007. Outbreak of chikungunya on Reunion Island: early clinical and laboratory features in 157 adult patients. Clin Infect Dis 44:1401–1407. https://doi.org/10.1086/517537.
17. Gérardin P, Couderc T, Bintner M, Tournebize P, Renouil M, Lémant J, Boisson V, Borgherini G, Staikowsky F, Schramm F, Lecuit M, Michault A, Encephalchik Study Group. 2016. Chikungunya virus-associated encephalitis: a cohort study on La Réunion Island, 2005–2009. Neurology 86:94–102. https://doi.org/10.1212/WNL.0000000000002234.
18. Borgherini G, Poubeau P, Jossaume A, Gouix A, Cotte L, Michault A, Arvin-Berod C, Paganin F. 2008. Persistent arthralgia associated with chikungunya virus: a study of 88 adult patients on Reunion Island. Clin Infect Dis 47:469–475. https://doi.org/10.1086/590003.
19. Sissoko D, Malvy D, Ezzedine K, Renault P, Moscetti F, Ledrans M, Pierre V. 2009. Post-epidemic chikungunya disease on Reunion Island: course of rheumatic manifestations and associated factors over a 15-month period. PLoS Negl Trop Dis 3:e389. https://doi.org/10.1371/journal.pntd.0000389.
20. Manimunda SP, Vijayachari P, Uppoor R, Sugunan AP, Singh SS, Rai SK, Sudeep AB, Muruganandam N, Chaitanya IK, Guruprasad DR. 2010.

Clinical progression of chikungunya fever during acute and chronic arthritic stages and the changes in joint morphology as revealed by imaging. Trans R Soc Trop Med Hyg 104:392–399. https://doi.org/10.1016/j.trstmh.2010.01.011.
21. Schilte C, Staikowsky F, Staikovsky F, Couderc T, Madec Y, Carpentier F, Kassab S, Albert ML, Lecuit M, Michault A. 2013. Chikungunya virus-associated long-term arthralgia: a 36-month prospective longitudinal study. PLoS Negl Trop Dis 7:e2137. https://doi.org/10.1371/journal.pntd.0002137.
22. Miner JJ, Aw Yeang HX, Fox JM, Taffner S, Malkova ON, Oh ST, Kim AHJ, Diamond MS, Lenschow DJ, Yokoyama WM. 2015. Brief report: chikungunya viral arthritis in the United States: a mimic of seronegative rheumatoid arthritis. Arthritis Rheumatol 67:1214–1220. https://doi.org/10.1002/art.39027.
23. Chang AY, Martins KAO, Encinales L, Reid SP, Acuña M, Encinales C, Matranga CB, Pacheco N, Cure C, Shukla B, Arteta TR, Amdur R, Cazares LH, Gregory M, Ward MD, Porras A, Mendoza AR, Dong L, Kenny T, Brueggemann E, Downey LG, Kamalapathy P, Lichtenberger P, Falls O, Simon GL, Bethony JM, Firestein GS. 2018. Chikungunya arthritis mechanisms in the Americas. Arthritis Rheumatol 70:585–593. https://doi.org/10.1002/art.40383.
24. Waymouth HE, Zoutman DE, Towheed TE. 2013. Chikungunya-related arthritis: case report and review of the literature. Semin Arthritis Rheum 43:273–278. https://doi.org/10.1016/j.semarthrit.2013.03.003.
25. Chopra A, Saluja M, Venugopalan A. 2014. Effectiveness of chloroquine and inflammatory cytokine response in patients with early persistent musculoskeletal pain and arthritis following chikungunya virus infection. Arthritis Rheumatol 66:319–326. https://doi.org/10.1002/art.38221.
26. Venugopalan A, Ghorpade RP, Chopra A. 2014. Cytokines in acute chikungunya. PLoS One 9:e111305. https://doi.org/10.1371/journal.pone.0111305.
27. Foissac M, Javelle E, Ray S, Guerin B, Simon F. 2015. Post-chikungunya rheumatoid arthritis, Saint Martin. Emerg Infect Dis 21:530–532. https://doi.org/10.3201/eid2103.141397.
28. Blettery M, Brunier L, Polomat K, Moinet F, Deligny C, Arfi S, Jean-Baptiste G, De Bandt M. 2016. Brief report: management of chronic post-chikungunya rheumatic disease: the Martinican experience: chronic post-chikungunya rheumatic disease. Arthritis Rheumatol 68:2817–2824. https://doi.org/10.1002/art.39775.
29. Mogami R, Pereira Vaz JL, de Fátima Barcelos Chagas Y, de Abreu MM, Torezani RS, de Almeida Vieira A, Junqueira Filho EA, Barbosa YB, Carvalho ACP, Lopes AJ. 2018. Ultrasonography of hands and wrists in the diagnosis of complications of chikungunya fever: hand and wrist complications in chikungunya fever. J Ultrasound Med 37:511–520. https://doi.org/10.1002/jum.14344.
30. Hoarau J-J, Jaffar Bandjee M-C, Krejbich Trotot P, Das T, Li-Pat-Yuen G, Dassa B, Denizot M, Guichard E, Ribera A, Henni T, Tallet F, Moiton MP, Gauzère BA, Bruniquet S, Jaffar Bandjee Z, Morbidelli P, Martigny G, Jolivet M, Gay F, Grandadam M, Tolou H, Vieillard V, Debré P, Autran B, Gasque P. 2010. Persistent chronic inflammation and infection by chikungunya arthritogenic alphavirus in spite of a robust host immune response. J Immunol 184:5914–5927. https://doi.org/10.4049/jimmunol.0900255.
31. Ozden S, Huerre M, Riviere J-P, Coffey LL, Afonso PV, Mouly V, de Monredon J, Roger J-C, Amrani ME, Yvin J-L, Jaffar M-C, Frenkiel M-P, Sourisseau M, Schwartz O, Butler-Browne G, Desprès P, Gessain A, Ceccaldi P-E. 2007. Human muscle satellite cells as targets of chikungunya virus infection. PLoS One 2:e527. https://doi.org/10.1371/journal.pone.0000527.
32. Hawman DW, Fox JM, Ashbrook AW, May NA, Schroeder KMS, Torres RM, Crowe JE, Jr, Dermody TS, Diamond MS, Morrison TE. 2016. Pathogenic chikungunya virus evades B cell responses to establish persistence. Cell Rep 16:1326–1338. https://doi.org/10.1016/j.celrep.2016.06.076.
33. Hawman DW, Stoermer KA, Montgomery SA, Pal P, Oko L, Diamond MS, Morrison TE. 2013. Chronic joint disease caused by persistent chikungunya virus infection is controlled by the adaptive immune response. J Virol 87:13878–13888. https://doi.org/10.1128/JVI.02666-13.
34. Poo YS, Rudd PA, Gardner J, Wilson JAC, Larcher T, Colle M-A, Le TT, Nakaya HI, Warrilow D, Allcock R, Bielefeldt-Ohmann H, Schroder WA, Khromykh AA, Lopez JA, Suhrbier A. 2014. Multiple immune factors are involved in controlling acute and chronic chikungunya virus infection. PLoS Negl Trop Dis 8:e3354. https://doi.org/10.1371/journal.pntd.0003354.
35. Uhrlaub JL, Pulko V, DeFilippis VR, Broeckel R, Streblow DN, Coleman GD, Park BS, Lindo JF, Vickers I, Anzinger JJ, Nikolich-Žugich J. 2016. Dysregulated TGF-β production underlies the age-related vulnerability to chikungunya virus. PLoS Pathog 12:e1005891. https://doi.org/10.1371/journal.ppat.1005891.
36. Young AR, Locke MC, Cook LE, Hiller BE, Zhang R, Hedberg ML, Monte KJ, Veis DJ, Diamond MS, Lenschow DJ. 2019. Dermal and muscle fibroblasts and skeletal myofibers survive chikungunya virus infection and harbor persistent RNA. PLoS Pathog 15:e1007993. https://doi.org/10.1371/journal.ppat.1007993.
37. Goh LYH, Hobson-Peters J, Prow NA, Gardner J, Bielefeldt-Ohmann H, Suhrbier A, Hall RA. 2015. Monoclonal antibodies specific for the capsid protein of chikungunya virus suitable for multiple applications. J Gen Virol 96:507–512. https://doi.org/10.1099/jgv.0.000002.
38. Labadie K, Larcher T, Joubert C, Mannioui A, Delache B, Brochard P, Guigand L, Dubreil L, Lebon P, Verrier B, de Lamballerie X, Suhrbier A, Cherel Y, Le Grand R, Roques P. 2010. Chikungunya disease in nonhuman primates involves long-term viral persistence in macrophages. J Clin Invest 120:894–906. https://doi.org/10.1172/JCI40104.
39. Messaoudi I, Vomaske J, Totonchy T, Kreklywich CN, Haberthur K, Springgay L, Brien JD, Diamond MS, DeFilippis VR, Streblow DN. 2013. Chikungunya virus infection results in higher and persistent viral replication in aged rhesus macaques due to defects in anti-viral immunity. PLoS Negl Trop Dis 7:e2343. https://doi.org/10.1371/journal.pntd.0002343.
40. Wauquier N, Becquart P, Nkoghe D, Padilla C, Ndjoyi-Mbiguino A, Leroy EM. 2011. The acute phase of chikungunya virus infection in humans is associated with strong innate immunity and T CD8 cell activation. J Infect Dis 204:115–123. https://doi.org/10.1093/infdis/jiq006.
41. Hoarau J-J, Gay F, Pellé O, Samri A, Jaffar-Bandjee M-C, Gasque P, Autran B. 2013. Identical strength of the T cell responses against E2, nsP1 and capsid CHIKV proteins in recovered and chronic patients after the epidemics of 2005–2006 in La Reunion Island. PLoS One 8:e84695. https://doi.org/10.1371/journal.pone.0084695.
42. Morrison TE, Oko L, Montgomery SA, Whitmore AC, Lotstein AR, Gunn BM, Elmore SA, Heise MT. 2011. A mouse model of chikungunya virus-induced musculoskeletal inflammatory disease. Am J Pathol 178:32–40. https://doi.org/10.1016/j.ajpath.2010.11.018.
43. Gardner J, Anraku I, Le TT, Larcher T, Major L, Roques P, Schroder WA, Higgs S, Suhrbier A. 2010. Chikungunya virus arthritis in adult wild-type mice. J Virol 84:8021–8032. https://doi.org/10.1128/JVI.02603-09.
44. Burrack KS, Montgomery SA, Homann D, Morrison TE. 2015. CD8$^+$ T cells control Ross River virus infection in musculoskeletal tissues of infected mice. J Immunol 194:678–689. https://doi.org/10.4049/jimmunol.1401833.
45. Burrack KS, Tan JJL, McCarthy MK, Her Z, Berger JN, Ng LFP, Morrison TE. 2015. Myeloid cell Arg1 inhibits control of arthritogenic alphavirus infection by suppressing antiviral T cells. PLoS Pathog 11:e1005191. https://doi.org/10.1371/journal.ppat.1005191.
46. McCarthy MK, Davenport BJ, Reynoso GV, Lucas ED, May NA, Elmore SA, Tamburini BA, Hickman HD, Morrison TE. 2018. Chikungunya virus impairs draining lymph node function by inhibiting HEV-mediated lymphocyte recruitment. JCI Insight 3:121100. https://doi.org/10.1172/jci.insight.121100.
47. Budd RC, Cerottini JC, Horvath C, Bron C, Pedrazzini T, Howe RC, MacDonald HR. 1987. Distinction of virgin and memory T lymphocytes. Stable acquisition of the Pgp-1 glycoprotein concomitant with antigenic stimulation. J Immunol 138:3120–3129.
48. Wherry EJ, Blattman JN, Murali-Krishna K, van der Most R, Ahmed R. 2003. Viral persistence alters CD8 T-cell immunodominance and tissue distribution and results in distinct stages of functional impairment. J Virol 77:4911–4927. https://doi.org/10.1128/jvi.77.8.4911-4927.2003.
49. Kaech SM, Wherry EJ. 2007. Heterogeneity and cell-fate decisions in effector and memory CD8$^+$ T cell differentiation during viral infection. Immunity 27:393–405. https://doi.org/10.1016/j.immuni.2007.08.007.
50. Muthumani K, Lankaraman KM, Laddy DJ, Sundaram SG, Chung CW, Sako E, Wu L, Khan A, Sardesai N, Kim JJ, Vijayachari P, Weiner DB. 2008. Immunogenicity of novel consensus-based DNA vaccines against chikungunya virus. Vaccine 26:5128–5134. https://doi.org/10.1016/j.vaccine.2008.03.060.
51. Broeckel RM, Haese N, Ando T, Dmitriev I, Kreklywich CN, Powers J, Denton M, Smith P, Morrison TE, Heise M, DeFilippis V, Messaoudi I,

Curiel DT, Streblow DN. 2019. Vaccine-induced skewing of T cell responses protects against chikungunya virus disease. Front Immunol 10:2563. https://doi.org/10.3389/fimmu.2019.02563.
52. Ross P, Holmes JC, Gojanovich GS, Hess PR. 2012. A cell-based MHC stabilization assay for the detection of peptide binding to the canine classical class I molecule, DLA-88. Vet Immunol Immunopathol 150:206–212. https://doi.org/10.1016/j.vetimm.2012.08.012.
53. Ljunggren H-G, Stam NJ, Öhlén C, Neefjes JJ, Höglund P, Heemels M-T, Bastin J, Schumacher TNM, Townsend A, Kärre K, Ploegh HL. 1990. Empty MHC class I molecules come out in the cold. Nature 346:476–480. https://doi.org/10.1038/346476a0.
54. Powis SJ, Townsend ARM, Deverson EV, Bastin J, Butcher GW, Howard JC. 1991. Restoration of antigen presentation to the mutant cell line RMA-S by an MHC-linked transporter. Nature 354:528–531. https://doi.org/10.1038/354528a0.
55. Lipford GB, Hoffman M, Wagner H, Heeg K. 1993. Primary in vivo responses to ovalbumin. Probing the predictive value of the Kb binding motif. J Immunol 150:1212–1222.
56. Rötzschke O, Falk K, Stevanovic S, Jung G, Walden P, Rammensee H-G. 1991. Exact prediction of a natural T cell epitope. Eur J Immunol 21:2891–2894. https://doi.org/10.1002/eji.1830211136.
57. Schulz M, Aichele P, Vollenweider M, Bobe FW, Cardinaux F, Hengartner H, Zinkernagel RM. 1989. Major histocompatibility complex-dependent T cell epitopes of lymphocytic choriomeningitis virus nucleoprotein and their protective capacity against viral disease. Eur J Immunol 19:1657–1667. https://doi.org/10.1002/eji.1830190921.
58. Klavinskis LS, Whitton JL, Joly E, Oldstone M. 1990. Vaccination and protection from a lethal viral infection: identification, incorporation, and use of a cytotoxic T lymphocyte glycoprotein epitope. Virology 178:393–400. https://doi.org/10.1016/0042-6822(90)90336-P.
59. Hudrisier D, Oldstone MBA, Gairin JE. 1997. The signal sequence of lymphocytic choriomeningitis virus contains an immunodominant cytotoxic T cell epitope that is restricted by both H-2D^b and H-2K^b molecules. Virology 234:62–73. https://doi.org/10.1006/viro.1997.8627.
60. Knudsen ML, Ljungberg K, Kakoulidou M, Kostic L, Hallengärd D, García-Arriaza J, Merits A, Esteban M, Liljeström P. 2014. Kinetic and phenotypic analysis of CD8$^+$ T cell responses after priming with alphavirus replicons and homologous or heterologous booster immunizations. J Virol 88:12438–12451. https://doi.org/10.1128/JVI.02223-14.
61. Wherry EJ, Ha S-J, Kaech SM, Haining WN, Sarkar S, Kalia V, Subramaniam S, Blattman JN, Barber DL, Ahmed R. 2007. Molecular signature of CD8$^+$ T cell exhaustion during chronic viral infection. Immunity 27:670–684. https://doi.org/10.1016/j.immuni.2007.09.006.
62. Jin H-T, Anderson AC, Tan WG, West EE, Ha S-J, Araki K, Freeman GJ, Kuchroo VK, Ahmed R. 2010. Cooperation of Tim-3 and PD-1 in CD8 T-cell exhaustion during chronic viral infection. Proc Natl Acad Sci U S A 107:14733–14738. https://doi.org/10.1073/pnas.1009731107.
63. Richter K, Agnellini P, Oxenius A. 2010. On the role of the inhibitory receptor LAG-3 in acute and chronic LCMV infection. Int Immunol 22:13–23. https://doi.org/10.1093/intimm/dxp107.
64. Betts MR, Brenchley JM, Price DA, De Rosa SC, Douek DC, Roederer M, Koup RA. 2003. Sensitive and viable identification of antigen-specific CD8$^+$ T cells by a flow cytometric assay for degranulation. J Immunol Methods 281:65–78. https://doi.org/10.1016/s0022-1759(03)00265-5.
65. Wolint P, Betts MR, Koup RA, Oxenius A. 2004. Immediate cytotoxicity but not degranulation distinguishes effector and memory subsets of CD8$^+$ T cells. J Exp Med 199:925–936. https://doi.org/10.1084/jem.20031799.
66. Harty JT, Tvinnereim AR, White DW. 2000. CD8$^+$ T cell effector mechanisms in resistance to infection. Annu Rev Immunol 18:275–308. https://doi.org/10.1146/annurev.immunol.18.1.275.
67. Chen W, Masterman K-A, Basta S, Haeryfar SMM, Dimopoulos N, Knowles B, Bennink JR, Yewdell JW. 2004. Cross-priming of CD8$^+$ T cells by viral and tumor antigens is a robust phenomenon. Eur J Immunol 34:194–199. https://doi.org/10.1002/eji.200324257.
68. Sigal LJ, Crotty S, Andino R, Rock KL. 1999. Cytotoxic T-cell immunity to virus-infected non-haematopoietic cells requires presentation of exogenous antigen. Nature 398:77–80. https://doi.org/10.1038/18038.
69. Rock KL, Gamble S, Rothstein L. 1990. Presentation of exogenous antigen with class I major histocompatibility complex molecules. Science 249:918–921. https://doi.org/10.1126/science.2392683.
70. Hildner K, Edelson BT, Purtha WE, Diamond M, Matsushita H, Kohyama M, Calderon B, Schraml B, Unanue ER, Diamond MS, Schreiber RD, Murphy TL, Murphy KM. 2008. Batf3 deficiency reveals a critical role for CD8α^+ dendritic cells in cytotoxic T cell immunity. Science 322:1097–1100. https://doi.org/10.1126/science.1164206.
71. Edelson BT, Kc W, Juang R, Kohyama M, Benoit LA, Klekotka PA, Moon C, Albring JC, Ise W, Michael DG, Bhattacharya D, Stappenbeck TS, Holtzman MJ, Sung S-S, Murphy TL, Hildner K, Murphy KM. 2010. Peripheral CD103+ dendritic cells form a unified subset developmentally related to CD8α^+ conventional dendritic cells. J Exp Med 207:823–836. https://doi.org/10.1084/jem.20091627.
72. Dudziak D, Kamphorst AO, Heidkamp GF, Buchholz VR, Trumpfheller C, Yamazaki S, Cheong C, Liu K, Lee H-W, Park CG, Steinman RM, Nussenzweig MC. 2007. Differential antigen processing by dendritic cell subsets in vivo. Science 315:107–111. https://doi.org/10.1126/science.1136080.
73. den Haan JMM, Lehar SM, Bevan MJ. 2000. Cd8$^+$ but not Cd8$^-$ dendritic cells cross-prime cytotoxic T cells in vivo. J Exp Med 192:1685–1696. https://doi.org/10.1084/jem.192.12.1685.
74. Theisen DJ, Davidson JT, Briseño CG, Gargaro M, Lauron EJ, Wang Q, Desai P, Durai V, Bagadia P, Brickner JR, Beatty WL, Virgin HW, Gillanders WE, Mosammaparast N, Diamond MS, Sibley LD, Yokoyama W, Schreiber RD, Murphy TL, Murphy KM. 2018. WDFY4 is required for cross-presentation in response to viral and tumor antigens. Science 362:694–699. https://doi.org/10.1126/science.aat5030.
75. Fung-Leung WP, Kündig TM, Zinkernagel RM, Mak TW. 1991. Immune response against lymphocytic choriomeningitis virus infection in mice without CD8 expression. J Exp Med 174:1425–1429. https://doi.org/10.1084/jem.174.6.1425.
76. Matloubian M, Concepcion RJ, Ahmed R. 1994. CD4$^+$ T cells are required to sustain CD8+ cytotoxic T-cell responses during chronic viral infection. J Virol 68:8056–8063. https://doi.org/10.1128/JVI.68.12.8056-8063.1994.
77. Zajac AJ, Blattman JN, Murali-Krishna K, Sourdive DJD, Suresh M, Altman JD, Ahmed R. 1998. Viral immune evasion due to persistence of activated T cells without effector function. J Exp Med 188:2205–2213. https://doi.org/10.1084/jem.188.12.2205.
78. Doherty PC, Hou S, Southern PJ. 1993. Lymphocytic choriomeningitis virus induces a chronic wasting disease in mice lacking class I major histocompatibility complex glycoproteins. J Neuroimmunol 46:11–17. https://doi.org/10.1016/0165-5728(93)90228-Q.
79. Stamm A, Valentine L, Potts R, Premenko-Lanier M. 2012. An intermediate dose of LCMV clone 13 causes prolonged morbidity that is maintained by CD4$^+$ T cells. Virology 425:122–132. https://doi.org/10.1016/j.virol.2012.01.005.
80. Alam SM, Travers PJ, Wung JL, Nasholds W, Redpath S, Jameson SC, Gascoigne N. 1996. T-cell-receptor affinity and thymocyte positive selection. Nature 381:616–620. https://doi.org/10.1038/381616a0.
81. Ahonen CL, Doxsee CL, McGurran SM, Riter TR, Wade WF, Barth RJ, Vasilakos JP, Noelle RJ, Kedl RM. 2004. Combined TLR and CD40 triggering induces potent CD8$^+$ T cell expansion with variable dependence on type I IFN. J Exp Med 199:775–784. https://doi.org/10.1084/jem.20031591.
82. Teo T-H, Lum F-M, Claser C, Lulla V, Lulla A, Merits A, Renia L, Ng L. 2013. A pathogenic role for CD4$^+$ T cells during chikungunya virus infection in mice. J Immunol 190:259–269. https://doi.org/10.4049/jimmunol.1202177.
83. Broeckel R, Fox JM, Haese N, Kreklywich CN, Sukulpovi-Petty S, Legasse A, Smith PP, Denton M, Corvey C, Krishnan S, Colgin LMA, Ducore RM, Lewis AD, Axthelm MK, Mandron M, Cortez P, Rothblatt J, Rao E, Focken I, Carter K, Sapparapau G, Crowe JE, Jr, Diamond MS, Streblow DN. 2017. Therapeutic administration of a recombinant human monoclonal antibody reduces the severity of chikungunya virus disease in rhesus macaques. PLoS Negl Trop Dis 11:e0005637. https://doi.org/10.1371/journal.pntd.0005637.
84. Chu H, Das SC, Fuchs JF, Suresh M, Weaver SC, Stinchcomb DT, Partidos CD, Osorio JE. 2013. Deciphering the protective role of adaptive immunity to CHIKV/IRES a novel candidate vaccine against chikungunya in the A129 mouse model. Vaccine 31:3353–3360. https://doi.org/10.1016/j.vaccine.2013.05.059.
85. Hallengärd D, Kakoulidou M, Lulla A, Kümmerer BM, Johansson DX, Mutso M, Lulla V, Fazakerley JK, Roques P, Le Grand R, Merits A, Liljeström P. 2014. Novel attenuated chikungunya vaccine candidates elicit protective immunity in C57BL/6 mice. J Virol 88:2858–2866. https://doi.org/10.1128/JVI.03453-13.
86. Hallengärd D, Lum F-M, Kümmerer BM, Lulla A, Lulla V, García-Arriaza J, Fazakerley JK, Roques P, Le Grand R, Merits A, Ng LFP, Esteban M,

Liljeström P. 2014. Prime-boost immunization strategies against chikungunya virus. J Virol 88:13333–13343. https://doi.org/10.1128/JVI.01926-14.
87. García-Arriaza J, Cepeda V, Hallengärd D, Sorzano CÓS, Kümmerer BM, Liljeström P, Esteban M. 2014. A novel poxvirus-based vaccine, MVA-CHIKV, is highly immunogenic and protects mice against chikungunya infection. J Virol 88:3527–3547. https://doi.org/10.1128/JVI.03418-13.
88. Erasmus JH, Auguste AJ, Kaelber JT, Luo H, Rossi SL, Fenton K, Leal G, Kim DY, Chiu W, Wang T, Frolov I, Nasar F, Weaver SC. 2017. A chikungunya fever vaccine utilizing an insect-specific virus platform. Nat Med 23:192–199. https://doi.org/10.1038/nm.4253.
89. Chattopadhyay A, Wang E, Seymour R, Weaver SC, Rose JK. 2013. A chimeric vesiculo/alphavirus is an effective alphavirus vaccine. J Virol 87:395–402. https://doi.org/10.1128/JVI.01860-12.
90. Wherry EJ. 2011. T cell exhaustion. Nat Immunol 12:492–499. https://doi.org/10.1038/ni.2035.
91. Dias CNDS, Gois BM, Lima VS, Guerra-Gomes IC, Araújo JMG, Gomes JDAS, Araújo DAM, Medeiros IA, de Azevedo FDLAA, Veras RC, Janebro DI, do Amaral IPG, Keesen TSL. 2018. Human CD8 T-cell activation in acute and chronic chikungunya infection. Immunology 155:499–504. https://doi.org/10.1111/imm.12992.
92. Walsh CM, Matloubian M, Liu CC, Ueda R, Kurahara CG, Christensen JL, Huang MT, Young JD, Ahmed R, Clark WR. 1994. Immune function in mice lacking the perforin gene. Proc Natl Acad Sci U S A 91:10854–10858. https://doi.org/10.1073/pnas.91.23.10854.
93. Kägi D, Ledermann B, Bürki K, Seiler P, Odermatt B, Olsen KJ, Podack ER, Zinkernagel RM, Hengartner H. 1994. Cytotoxicity mediated by T cells and natural killer cells is greatly impaired in perforin-deficient mice. Nature 369:31–37. https://doi.org/10.1038/369031a0.
94. Barber DL, Wherry EJ, Ahmed R. 2003. Cutting edge: rapid in vivo killing by memory CD8 T cells. J Immunol 171:27–31. https://doi.org/10.4049/jimmunol.171.1.27.
95. Russell JH, Ley TJ. 2002. Lymphocyte-mediated cytotoxicity. Annu Rev Immunol 20:323–370. https://doi.org/10.1146/annurev.immunol.20.100201.131730.
96. Blum JS, Wearsch PA, Cresswell P. 2013. Pathways of antigen processing. Annu Rev Immunol 31:443–473. https://doi.org/10.1146/annurev-immunol-032712-095910.
97. Vremec D, Shortman K. 1997. Dendritic cell subtypes in mouse lymphoid organs: cross-correlation of surface markers, changes with incubation, and differences among thymus, spleen, and lymph nodes. J Immunol 159:565–573.
98. Shortman K, Heath WR. 2010. The CD8$^+$ dendritic cell subset. Immunol Rev 234:18–31. https://doi.org/10.1111/j.0105-2896.2009.00870.x.
99. National Research Council. 2011. Guide for the care and use of laboratory animals, 8th ed. National Academies Press, Washington, DC.
100. American Veterinary Medical Association. 2020. Guidelines for the euthanasia of animals. American Veterinary Medical Association, Schaumburg, IL.
101. Ashbrook AW, Burrack KS, Silva LA, Montgomery SA, Heise MT, Morrison TE, Dermody TS. 2014. Residue 82 of the chikungunya virus E2 attachment protein modulates viral dissemination and arthritis in mice. J Virol 88:12180–12192. https://doi.org/10.1128/JVI.01672-14.
102. Eberlein J, Davenport B, Nguyen TT, Victorino F, Sparwasser T, Homann D. 2012. Multiple layers of CD80/86-dependent costimulatory activity regulate primary, memory, and secondary lymphocytic choriomeningitis virus-specific T cell immunity. J Virol 86:1955–1970. https://doi.org/10.1128/JVI.05949-11.
103. Barchet W, Oehen S, Klenerman P, Wodarz D, Lloyd AL, Nowak MA, Hengartner H, Zinkernagel RM, Ehl S. 2000. Direct quantitation of rapid elimination of viral antigen-positive lymphocytes by antiviral CD8$^+$ T cells in vivo. Eur J Immunol 8:1356–1363.
104. Ledgerwood LG, Lal G, Zhang N, Garin A, Esses SJ, Ginhoux F, Merad M, Peche H, Lira SA, Ding Y, Yang Y, He X, Schuchman EH, Allende ML, Ochando JC, Bromberg JS. 2008. The sphingosine 1-phosphate receptor 1 causes tissue retention by inhibiting the entry of peripheral tissue T lymphocytes into afferent lymphatics. Nat Immunol 9:42–53. https://doi.org/10.1038/ni1534.
105. Stoermer KA, Burrack A, Oko L, Montgomery SA, Borst LB, Gill RG, Morrison TE. 2012. Genetic ablation of arginase 1 in macrophages and neutrophils enhances clearance of an arthritogenic alphavirus. J Immunol 189:4047–4059. https://doi.org/10.4049/jimmunol.1201240.
106. McCausland MM, Crotty S. 2008. Quantitative PCR technique for detecting lymphocytic choriomeningitis virus in vivo. J Virol Methods 147:167–176. https://doi.org/10.1016/j.jviromet.2007.08.025.